Atmósfera 40, 281-312 (2026)
https://doi.org/10.20937/ATM.53548

Evaluating the dual role of African dust and water vapor in influencing atmospheric stability across the Caribbean Islands

Mohammed S. ABED[1]*, Ahmed F. HASSOON[2] and Aqeel D. SALMAN[3]

[1] *College of Science, Department of Biology, AL-Qassim Green University, Babel, Iraq.*
[2] *College of Science, Department of Atmospheric Sciences, Mustansirya University, Baghdad, Iraq.*
[3] *College of Renewable Energy & Environmental Science, Department of Environmental Science, AL-Kharkh University of Science, Baghdad, Iraq.*
*Corresponding author; email: mohammed.sh@science.uoqasim.edu.iq

Received: October 11, 2025; Accepted: May 12, 2026

RESUMEN

Se investiga el efecto termodinámico de la Capa de Aire Sahariana (SAL, por su sigla en inglés) sobre la estabilidad convectiva en la cuenca del Caribe mediante el análisis estadístico de la profundidad óptica de aerosoles (AOD), el vapor de agua y la energía potencial convectiva disponible (CAPE) sobre Barbados, Guadalupe, Puerto Rico y las Islas Caimán. Este trabajo cuantifica los controles jerárquicos sobre la inestabilidad atmosférica mediante el análisis de las correlaciones en regímenes de polvo y de bajo polvo, así como de los cambios porcentuales en la CAPE bajo el forzamiento combinado de polvo y vapor de agua. Los resultados muestran que el vapor de agua, que presenta relaciones positivas sólidas y frecuentemente significativas con la CAPE, es la principal causa de la convección. Por el contrario, las correlaciones AOD-CAPE suelen ser insignificantes, lo que indica que la carga de polvo por sí sola no es un buen predictor lineal del potencial convectivo. Por el contrario, el polvo actúa como un importante modulador secundario; al combinarse con el vapor de agua, reduce continuamente la CAPE en cada sitio, con disminuciones promedio entre −0.76 y −18.11 %. Las mayores reducciones se producen durante la noche en Barbados, lo que pone de relieve la importancia de la proximidad del polvo y la ausencia de forzamiento térmico durante el día. Además, el polvo actúa como un "desacoplador" que introduce no linealidad y, en algunas situaciones, oscurece estadísticamente la relación entre la humedad y la CAPE, alterando así la relación humedad-convección. Estos resultados demuestran que el potencial convectivo de la humedad ambiental se ve contrarrestado por el efecto estabilizador unidireccional del polvo sahariano en la atmósfera tropical. Los hallazgos resaltan la necesidad de utilizar parametrizaciones que consideren el polvo en los modelos climáticos regionales y mediciones de aerosoles con resolución vertical para mejorar los pronósticos de lluvia, sequía y actividad de tormentas tropicales en todo el Caribe.

ABSTRACT

The thermodynamic effect of the Saharan Air Layer (SAL) on convective stability in the Caribbean Basin is investigated through statistical analysis of aerosol optical depth (AOD), water vapor, and convective available potential energy (CAPE) over Barbados, Guadeloupe, Puerto Rico, and the Cayman Islands. This work quantifies the hierarchical controls on atmospheric instability by looking at correlations under dusty and low-dust regimes and percentage changes in CAPE under combined dust-water vapor forcing. The results show that water vapor, which has strong and often significant positive relationships with CAPE, is the primary driver of convection. In contrast, AOD-CAPE correlations are usually insignificant, indicating that dust loading by itself is not a good linear predictor of convective potential. Conversely, dust serves as an important secondary modulator; when combined with water vapor, it continuously reduces CAPE at every site, with average decreases ranging from −0.76 to –18.11%. The largest reductions occur at night in Barbados, highlighting

© 2026 Universidad Nacional Autónoma de México, Instituto de Ciencias de la Atmósfera y Cambio Climático.
This is an open access article under the CC BY-NC License (http://creativecommons.org/licenses/by-nc/4.0/).

the significance of dust proximity and the absence of daytime thermal forcing. Furthermore, dust acts as a "decoupler", introducing non-linearity and, in some situations, statistically obscuring the relationship between moisture and CAPE, thereby altering the moisture-convection relationship. These results demonstrate that the convective potential offered by ambient moisture is counteracted by the unidirectional stabilizing effect of Saharan dust on the tropical atmosphere. The findings highlight the necessity of using dust-aware parameterizations in regional climate models and vertically resolved aerosol measurements to enhance forecasts of rainfall, drought, and tropical storm activity throughout the Caribbean.

Keywords: Saharan dust, water vapor, stability, CAPE, CIN, Caribbean Islands.

1. Introduction

The main source of dust in the atmosphere is thought to be the Sahara Desert in northern Africa, which accounts for about half of the world's annual dust emissions, ranging from 400 to 2200 Tg yr^{-1} (Huneeus et al., 2011; Kok et al., 2021). The greatest amount of dust is lofted into the atmosphere and travels thousands of miles across the Atlantic Ocean by the impact of dominating winds.

Due to dry convection, the Saharan Air Layer (SAL) is generally hot, dry, and deeply mixed over the African continent. The long-term presence of Saharan dust in the atmosphere allows dust particles to interact with radiation. This interaction can alter radiative heating and cooling rates across various spatial and temporal scales by absorbing, scattering, and re-emitting long-wave (LW) and short-wave (SW) radiation. Saharan dust is a significant contributor to thermodynamic processes such as atmospheric instability, in which dust can affect tropical cyclones, atmospheric circulations, and precipitation formation (Chen et al., 2021; Xi et al., 2026).

Dynamic and turbulent processes have been considered crucial factors in dust transfer within the SAL (Rodakoviski, 2024). Despite the fact that earlier studies have concentrated on the radiative effects of transported SAL over oceans (e.g., Zhu et al., 2007), turbulent processes inside the SAL can sustain dust large particles to remain in the atmosphere for a long time (Rodakoviski et al., 2023), and dust associated with water vapor establishes static unstable layers during dust transport (Gutleben and Groß, 2021). Other studies show that the vertical gradients of both dust and water vapor are much diminished within the convective boundary layer (CBL) and under extremely stable conditions (Giménez et al., 2010).

Previous literature on evaluating the combined effects of dust and water vapor on atmospheric stability has received limited attention, although a few studies have examined the effects of dust and water on SAL over the Atlantic (Barreto et al., 2022). Over land, Awoleye et al. (2025) investigate the dual role of moisture and dust over the coastlines of West Africa, indicating that integrated vapor is a key factor in the dynamic development of dust movement during summer. Earlier studies implemented by Mote et al. (2017) provide a significant alternative to researching convection by easterly waves in terms of the thermodynamics of Saharan dust and moisture in local convection throughout the summer (i.e., June), in addition to the effects of dust and water vapor. Over oceans, Xi et al. (2026) give a good example of Saharan dust impact on offshore instability (i.e., precipitation process) across the Atlantic, while Dunion and Velden (2004) look into the impact of SAL on Atlantic tropical cyclone activity, suggesting that lower convective available potential energy (CAPE) values are associated with increased atmospheric stability. Additionally, Flores et al. (2023) compare the impact of Saharan dust on convective inhibition and atmospheric stability over the northern tropical Atlantic in May 2007 to that over Caribbean Islands and African land. They show that dust prevents deep convection above the trade wind layer by exacerbating the temperature inversion and generating convection inhibition (CIN) over 0.5 km in the SAL.

Other previous work shows that SAL is accompanied by a substantial amount of water vapor rather than a dry layer. The observations of authors such as Durán-Quesada et al. (2010), Gutleben et al. (2019, 2020, 2022), and Ryder (2021) show that a moist atmospheric layer is present during dust transport across the Atlantic. This indicates that both the water vapor and dust may share the impact on radiative transfer and atmospheric stability during dust

transport over the Atlantic and, consequently, the Caribbean basin.

The objectives of this research are to quantify the ways in which dust and water vapor affect atmospheric stability and determine how the effects of water vapor and dust vary among the chosen islands.

2. Methodology

2.1 Study region and datasets: radiosonde observations

Four Caribbean Island regions—Barbados (case A; 13.1ºN, 59.6ºW; Guadeloupe (case B; 16.3ºN, 61.0ºW); Puerto Rico (case C), located in the Central-eastern Caribbean (18.2º N, 66.6º W); and the Cayman Islands (case D; 19.3º N, 81.4º W)—are situated in the western part of the Atlantic (Fig. 1). We used atmospheric profiles, including atmospheric pressure, geopotential height, temperature, potential temperature, water vapor, and relative humidity (Durre et al., 2006, 2018), from the Integrated Global Radiosonde Archive (IGRI) observations.

A total of 24 days were considered, including low-dust (June 9, 28; September 12-15) and dusty (May 18-19; June 1, 25-27), at 00:00 and 12:00 UTC in each study region. In some cases (Guadeloupe and Cayman), there was missing information (errors) in the relative humidity values, thus, relative humidity was computed in FORTRAN code using the formula

$$RH = \left(\frac{e}{e_s}\right) x\ 100\% \quad (1)$$

where vapor pressure (e) and saturated vapor pressure (e_s) were taken from the radiosonde datasets.

2.2 MODIS-Aqua and AERONET observations

In this work, dust intensity was quantified using a time-averaged map for aerosol optical depth (AOD) based on Moderate Resolution Imagining Spectrometer (MODIS)-Aqua satellite images (Schumacher et al., 2024). With a daily temporal resolution and a geographical resolution of 1º across land and ocean, MODIS-Aqua generates AOD globally. Also, we used time series of averaged MODIS-AOD at 0.55 μm to identify AOD values. In addition to AOD observations, we used Aerosol Robotic Network (AERONET) data (Buchard et al., 2015; Lurduy, 2021) as supplementary AOD to classify dust intensity for days that were not captured by MODIS measurements. AERONET generates AOD using a broad range of wavelengths of eight nominal standard aerosol wavelengths (340, 380, 440, 500, 675, 870, 1020, and 1640 nm), and it determines AOD values based on Rayleigh scattering calculations (Holben et al., 1998). AODs with longer wavelengths (675, 870, 1020, and 1640 nm) have less of an impact on AOD calculations than those with shorter wavelengths (340, 380, and 440 nm).

2.3 Research tools

To assess the impact of water vapor and dust on atmospheric stability, many indices were computed using radiosonde datasets. For each dust-event day, we considered radiosonde observations twice: at 00:00 and

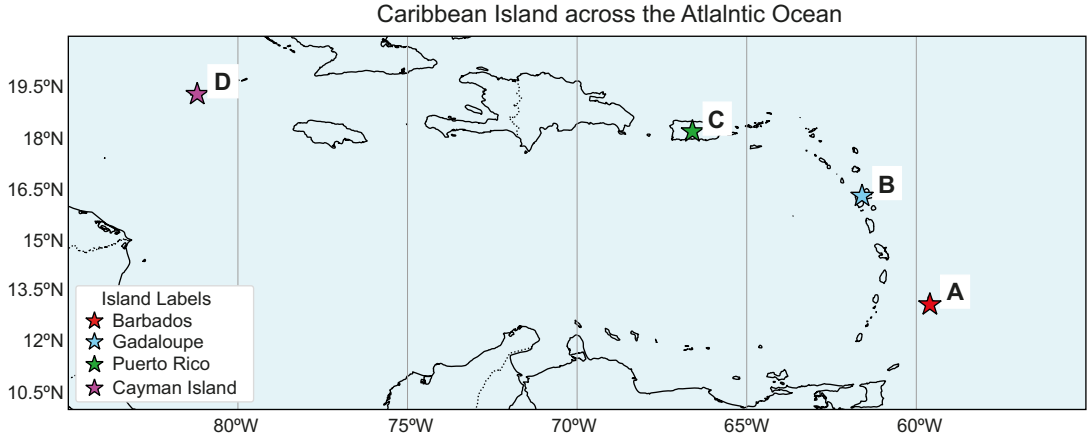

Fig. 1. Caribbean Islands include Barbados (A), Guadeloupe (B), Puerto Rico (C), and the Cayman Islands (D) over the Atlantic Ocean.

12:00 UTC. The impacts of dust and water vapor were assessed in our study, as we previously related to literature studies (i.e., dusty days characterized by high water vapor). We used the midlatitude-referenced water vapor profile (based on Anderson et al. [1986] and Gutleben et al. [2019]) for the summer period in the CAPE and CIN calculations to determine the individual effect of dust during this period (see Fig. S1 in the supplementary material). The reason for that is there is a big difference in referenced water vapor for these two cases, where the tropical one indicates a reference profile during wintertime, which is greater (way off) than both water vapor profiles for these times of dusty events at altitudes from the surface to about 3 km.

2.3.1 CAPE and CIN calculations

CAPE and CIN indices were calculated using radiosonde datasets to assess the effects of dust and water vapor on atmospheric stability in the Caribbean basin. These computations are performed once using water vapor from radiosonde data and again using referenced water vapor for each day of the dust event. Because CAPE and CIN quantify the buoyancy of an air parcel in the vertical, they have been regarded by prior research as accurate indicators of atmospheric instability in tropical convection (Khan et al., 2022). Holton (2004) and Linders and Saetra (2010) have demonstrated the mathematical computation of CAPE and CIN.

$$CAPE = \int_{zlfc}^{zel} g\left(\frac{T_{v,p} - T_{v,env}}{T_{v,env}}\right)dz \tag{2}$$

where *CAPE* is defined as the amount of convective energy in units of J kg^{-1} that potentially accelerates an air parcel to move vertically; $T_{v,p}$ and $T_{v,env}$ show the virtual temperatures for air parcels and the environment; and *zel* and *zlfc* indicate the height of the equilibrium level and the height of the level of free convection, respectively. The assumption of CAPE describes when the virtual temperature ($T_{v,p}$) of an air parcel lifted dry adiabatically from the surface to the lifted condensation level (LCL) or lifted moist adiabatically above this level, becomes equal or greater than $T_{v,env}$. Then, this expression is represented as an integration from *zlfc* to *zel*, for which $T_{v,env} - T_{v,p}$ is not equal to zero.

Therefore, CAPE calculates the positive amount of available potential energy for the convection process, where the larger value of CAPE indicates larger convection growth, thus leading to thunderstorms. In contrast, the negative energy that is represented as the opposite of CAPE is CIN, which is defined as the summation of negative energy from the surface to *zlfc* and can be expressed by the following formula:

$$CIN = \int_{zls}^{zlfc} g\left(\frac{T_{v,env} - T_{v,p}}{T_{v,env}}\right)dz \tag{3}$$

When a descended air parcel overcomes the negative buoyancy from its level between surface (*zls*) and free convection (*zlfc*), the integral formula of CIN is computed. In this work, we used a written FORTRAN 95 code to calculate the CAPE and CIN indices to evaluate the impacts of dust and water vapor on atmospheric stability over the Caribbean islands. Our method for calculating CAPE and CIN is comparable to that of Linders and Saetra (2010). We used radiosonde observations in Eqs. (2) and (3) to compute CAPE and CIN for statistical consideration and for convective energy evaluation in the vertical structure (differential CAPE and CIN calculations). Height (z), pressure (p), temperature (t), relative humidity (*RH*), potential temperature (θ), and water vapor (wv) were the atmospheric variables used in the code. A collection of formulas was used to build the FORTRAN code, and each computation adheres to the physical process of lifting an air parcel vertically (dry) and wet (adiabatically). The virtual temperature of the environment is represented by

$$T_{v,env} = th/(1000/p)^{0.2896} \tag{4}$$

whereas the virtual temperature of the lifted air parcel ($T_{v,p}$) was calculated using

$$T_{v,p} = t \times ([1 + wv]/0.622)/(1 + wv) \tag{5}$$

Also,

$$LCL = (20 + [te - 273.16]/5) \times (100 - RH) \tag{6}$$

can be used to compute the lifted condensation level. If $T_{v,p} > T_{v,env}$, the code will sign the CAPE area; if not, it will sign the CIN area and display the results.

The CAPE and CIN indices are computed for each location in order to assess the impact of dust and water vapor on atmospheric stability. To put it another

way, the presence of both dust and water vapor on days with high and low dust was taken into account when assessing the effects of dust and moisture on atmospheric stability. For the dust effect alone, CAPE and CIN were implemented by substituting a midlatitude-referenced water vapor profile based on both Anderson et al. (1986) and Gutleben et al. (2019) for water vapor profiles (i.e., water vapor based on radiosonde observations). We next computed CAPE and CIN using the modified water vapor profile that was produced for each research scenario. Since water vapor is introduced to the $T_{v,p}$ formula, it is visible that it is a very significant factor in evaluating CAPE and CIN calculations. Consequently, the values of CAPE and CIN in both situations will vary if the amount of water vapor in dust that coincides with moisture and dust alone varies with altitude.

3. Results

In preparation for presenting the findings, dusty event days included June 1, 25-27 (summer), and May 18-19, while June 9, 28, and September 12-15 were low-dust days. This categorization of dust-event days was then taken into account in the study.

3.1 Radiosonde observations

This section displays the meteorological profiles for the combined dust-and-water-vapor scenarios. All atmospheric profiles are shown in Figures S2-S7 in the supplementary material, including potential temperatures (a-d), relative humidity (e-h), and water vapor (i-l). Profiles for days June 1 and 9 are presented in Figure S2; Figure S3 shows results on June 25 and 28; Figure S4 shows profiles on June 26 and September 12; Figure S5 shows profiles on June 27 and September 13; Figure S6 shows results on May 18 and September 14, and Figure S7 presents results on May 19 and September 15. Letters A, B, C, and D stand for Barbados, Guadeloupe, Puerto Rico, and the Cayman Islands, respectively, and the first and second rows represent the atmospheric profiles at 00:00 and 12:00 UTC on each day. Black and blue lines display the vertical profiles for Barbados (A) and Guadeloupe (B), while green and red lines show Puerto Rico (C) and the Cayman Islands (D), respectively. Potential temperature profiles in Figures S2-S7 demonstrate steady rises over the vertical structure in all research cases. However, on dusty days such as June 25, the vertical structure of the potential temperature's inversion layer is situated between about 1.5 and 2 km, which exhibits a notable shift (increase) in the profile between these elevations, but the increase is lower on other days.

Relative humidity and water vapor mass mixing ratios show clear variations in the vertical atmospheric profiles. In the Caribbean Islands, this variance is associated with the inversion layer. For instance, observations over time show that relative humidity and water vapor structures differ between Barbados (black lines, case A) and Puerto Rico (green lines, case C); nonetheless, Puerto Rico exhibits the most significant variance among the Caribbean sites. Compared to Guadeloupe and Puerto Rico, Barbados had the highest relative humidity (between 1.5 and 3.5 km) on June 1, 25, and 9; however, the relationship flipped on June 28. Plots (e-h) and (i-l) in Figures S2 and S3 show why the potential temperature and water vapor profiles over Barbados (black lines) are greater than those over Puerto Rico (green lines), but they shifted back (decreased) on May 18 and 19 (Figs. S6 and S7). On the other hand, Cayman, which is positioned far from the African land, shows little difference in these profiles. Some data were missing due to errors in the radiosonde measurement platforms, such as in the Cayman Islands on June 25 and 28.

3.2 MODIS satellite observations

All satellite observations were related to the AOD measurements under dust conditions influenced by water vapor (scenario 1). Dust profiles over the Caribbean Islands vary, according to MODIS-Aqua measurements. The Caribbean islands' positions and the dynamic of wind impact can be used to explain this unpredictability. Daily averages of AOD on June 25, shown in Figure 2d, demonstrate that AOD values in Barbados, Guadeloupe, and Puerto Rico differ. Nevertheless, MODIS observations demonstrate good spatial identification of Saharan dust transport, with an intense spatial distribution at roughly 15º latitude across the Atlantic. AOD-satellite observations have good agreement with previous work in which dust has vertical and longitudinal variabilities over the Caribbean basin (Jury, 2017).

Over Puerto Rico, the daily averages of AOD on June 9 and 28 (Fig. 2a and b) reveal extremely low dust occurrences with some obvious values of

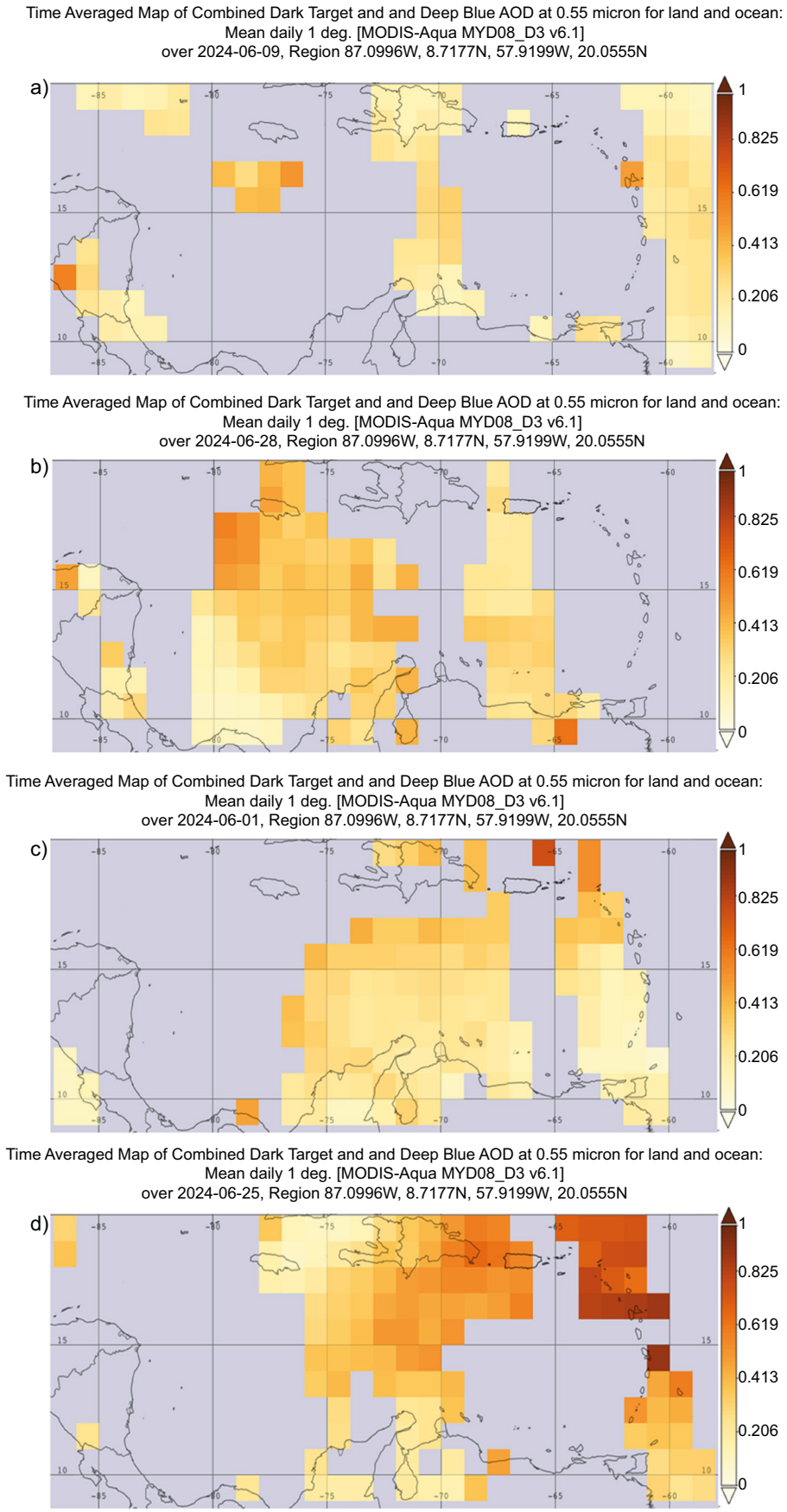

Fig. 2. Examples of daily time averages for low dust (June 9 and 28) and dusty (June 1 and 25) events taken from satellite observations for: (a, b) AOD based on MODIS-Aqua satellite observations at 0.55 μm for low dust; (c, d) AOD for dusty days. (AOD: aerosol optical depth.)

approximately 0.2 and 0.3 during these days, while values in Barbados are about 0.3; however, there is no clear value on June 28. Because of this, dust estimates from MODIS satellite observations in the Caribbean Islands vary greatly, with wind factors able to redirect dust movement across the Atlantic.

3.3 Impacts of both dust and water vapor on atmospheric stability

3.3.1 CAPE and CIN results

In this section, CAPE and CIN results are displayed for both scenarios (1 and 2). For scenario 1, Figure 3, and Figures S8 and S9 in the supplementary material show the vertical contributions of CIN (dashed lines) and CAPE (solid lines) computations at 00:00 UTC and 12:00 UTC for the cases of Barbados (black line), Guadeloupe (blue line), Puerto Rico (green line), and Cayman Islands (red line). The values of CAPE and CIN are represented in units of J kg^{-1} and are shown on the *y*-axis.

CAPE contributions are greatest in the upper troposphere (above 5 km) but continuously decrease from the surface up to about 3 km across all dates, stations, and time steps. The extensively distributed CAPE with the greatest instability was seen on June 1 and 25 (Fig. 3), June 26-27, and May 18-19 (Fig. S9). On the other hand, September values show steadier conditions across all four locations, especially on September 15. In general, the convective instability in Puerto Rico (green) and the Cayman Islands (red), which exhibit moderate contributions, is smaller than the CAPE values at Barbados and Guadeloupe. Even though Cayman's vertical CAPE is minimal, there is peak instability at some levels. In addition to the vertical CAPE contributions, Puerto Rico (green lines) shows the calmest (more stable) layer compared with other Caribbean regions, with its CAPE area longer and narrower at higher elevations.

The vertically integrated CAPE values with dust and moisture existences between the surface and up to 7 km linked with AOD values for all dates and times across the Caribbean Islands are shown in Table I. CAPE exhibits significant regional and temporal convective fluctuations, ranging from approximately 270 J kg^{-1} (Guadeloupe, June 9, 00:00 UTC) to over 2287 J kg^{-1} (Puerto Rico, May 18, 12:00 UTC). In Puerto Rico, late June and May have the highest CAPE values linked to high AOD (0.66). September values, on the other hand, exhibit low/moderate values (700-1635 J kg^{-1}) and are linked to the lowest AOD (0.1-0.2).

Tables II and III display Pearson correlation coefficients (r) and corresponding p-values for each study region at time 00:00 and 12:00 UTC in order to examine the relationship between AOD and CAPE during Saharan dust outbreaks. Overall, Table II shows a somewhat positive correlation between AOD and instability, suggesting that increased aerosol loading is associated with higher CAPE. Barbados exhibits extremely weak positive associations on dusty days ($r = 0.14$, $p = 0.70$ at 00:00 UTC; $r = 0.002$, $p = 0.99$ at 12:00 UTC). This suggests that, regardless of the time of day, AOD has no appreciable effect on CAPE in Barbados during dusty circumstances. Likewise, Guadeloupe has low correlations ($r = 0.16$, $p = 0.75$) at 12:00 UTC and positive correlations ($r = 0.21$, $p = 0.78$) at 00:00 UTC. These results are non-significant and indicate that dust loading does not consistently affect convective instability at Barbados and Guadeloupe, even though water vapor is present with AOD. At 00:00 UTC, the Puerto Rico site shows the largest positive correlation among all stations ($r = 0.52$, $p = 0.28$), whereas at 12:00 UTC it shows a significant correlation ($r = 0.33$, $p = 0.51$). Additionally, Cayman shows a mild negative correlation at 12:00 UTC ($r = -0.10$, $p = 0.01$), but an intriguing moderate positive correlation at 00:00 UTC ($r = 0.43$, $p = 0.46$). The moderate-to-strong correlation at 00:00 UTC indicates a physically meaningful positive association between dust aerosol loading and CAPE, possibly reflecting aerosol-induced thermodynamic modifications enhancing atmospheric instability, even though neither result reaches statistical significance.

To determine whether dust-convection interactions differ under cleaner atmospheric conditions than in dusty outbreaks, we calculated the r- and p-values for low-dust periods. In contrast to the obvious positive tendency during dust outbreaks, Table III shows primarily negative (reversal sign) correlations across the majority of study regions, indicating that under low aerosol loading, bigger AOD corresponds to lesser CAPE. The statistical findings indicate that the Guadeloupe, Puerto Rico, and Cayman sites contribute significantly to dust-convective interactions, even though Barbados shows a weak positive correlation ($r = 0.17$, $p = 0.88$ at 00:00 UTC;

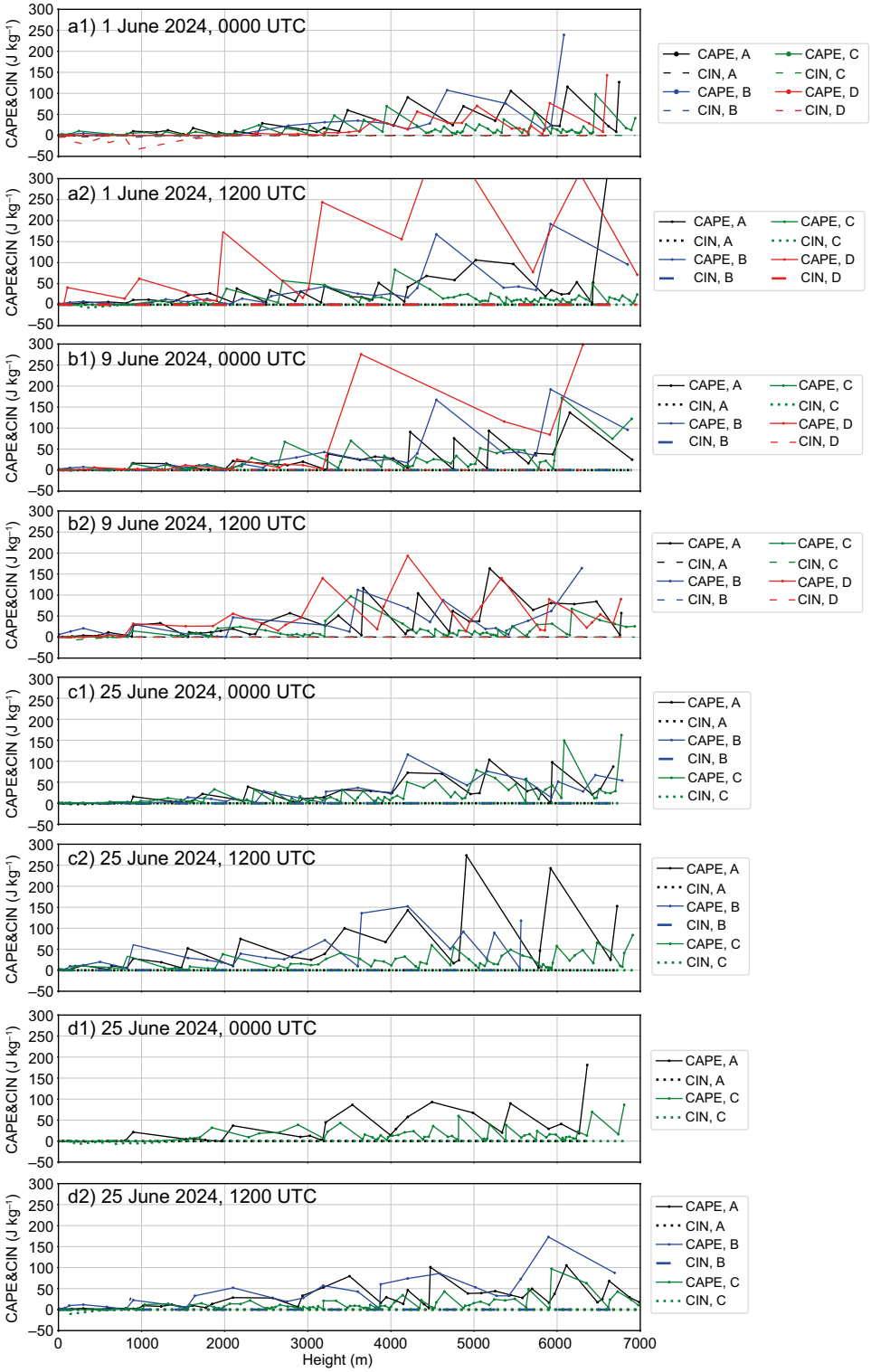

Fig. 3. CAPE and CIN vertical findings for the Caribbean Islands on June 1, 9, 25, and 28, 2024. Dust and water vapor were calculated for each case at 00:00 and 12:00 UTC (a1, b1, c1, d1, and a2, b2, c2, d2). CAPE values for Barbados, Guadeloupe, Puerto Rico, and the Cayman Islands are indicated by the solid black, blue, green, and red lines, respectively. CIN values are represented by dashed lines. Due to an inaccuracy in the relative humidity readings from radiosonde measurements, case (D) lacks CAPE or CIN values on days 25 and 28. (CAPE: convective available potential energy; CIN: convective inhibition.)

Table I. Integrated vertical CAPE (J kg^{-1}) values under dust and water vapor effects (scenario 1) for Barbados (case A), Guadeloupe (case B), Puerto Rico (case C), and Cayman Islands (case D) with AODs during low dust days (June 9 and 28 [summer] and September 12-15 [autumn]); and dusty days (May 18-19 and 1, June 25-27 [summer]) at 00:00 and 12:00 UTC.

Date, time (UTC)	Barbados		Guadeloupe		Puerto Rico		Cayman Islands	
	AOD	CAPE (J kg^{-1})	AOD	CAPE (J kg^{-1})	AOD	CAPE (J kg^{-1})	AOD	CAPE (J kg^{-1})
1 June, 00:00	0.1	883.9	0.2	640	0.4	1081.3	0.25	620.1
25 June, 00:00	0.3	830.9	0.5	668.2	0.55	1569.7	—	—
26 June, 00:00	0.4	1130	0.3	825	0.5	1137	0.3	1378
27 June, 00:00	0.2	1347	0.4	1097	0.3	1325	0.2	1170
18 May, 00:00	0.3	1076	0.3	—	0.14	1111	0.16	806
19 May, 00:00	0.3	1092	0.4	—	0.26	1124	0.23	944
1 June, 12:00	0.1	1292.6	0.23	878.6	0.3	1035.2	0.2	1861.9
25 June, 12:00	0.3	1415.6	0.66	1615	0.55	1398.2	—	—
26 June, 12:00	0.4	1414	0.4	843	0.4	1104	0.3	1199
27 June, 12:00	0.2	1423	0.3	1283	0.25	1039	0.2	856
18 May, 12:00	0.3	961	0.3	2256	0.4	2287	0.19	856
19 May, 12:00	0.3	1282	0.4	1307	0.45	1328	0.2	964
9 June, 00:00	0.2	747.6	0.3	270.8	0.14	1214.5	0.2	882.6
28 June, 00:00	0.2	837	—	—	0.12	945.5	—	—
12 Sep, 00:00	0.3	919	0.2	1104	0.1	822	0.1	1635
13 Sep, 00:00	0.2	1081	0.2	806	0.2	702	0.1	1181
14 Sep, 00:00	0.2	843	0.2	1041	0.2	818	0.2	1354
15 Sep, 00:00	0.2	974	0.2	1150	0.2	996	0.2	1311
9 June, 12:00	0.25	1283.4	0.25	833.5	0.13	872.3	—	—
28 June, 12:00	0.2	1101	0.13	971	0.1	962.7	—	—
12 Sep, 12:00	0.2	1377	0.2	1296	0.2	708	0.1	—
13 Sep, 12:00	0.2	1112	0.2	1186	0.2	998	0.1	956
14 Sep, 12:00	0.2	1182	0.2	1473	0.2	1035	0.2	1422
15 Sep, 12:00	0.2	1415	0.2	1331	0.2	808	0.2	—

AOD: aerosol optical depth; CAPE: convective available potential energy.

Table II. Statistical results between AOD and CAPE for dusty days during June and May 2024.

Sites/dusty days	r	p
Barbados (00:00 UTC)	0.14	0.7
Barbados (12:00 UTC)	0.002	0.9
Guadeloupe (00:00 UTC)	0.21	0.78
Guadeloupe (12:00 UTC)	0.16	0.75
Puerto Rico (00:00 UTC)	0.52	0.28
Puerto Rico (12:00 UTC)	0.33	0.51
Cayman Islands (00:00 UTC)	0.43	0.46
Cayman Islands (12:00 UTC)	–0.1	0.01

AOD: aerosol optical depth; CAPE: convective available potential energy.

Table III. Statistical results between AOD and CAPE for low dust during June and September 2024.

Sites/low dust	r	p
Barbados (00:00 UTC)	0.17	0.88
Barbados (12:00 UTC)	0.13	0.79
Guadeloupe (00:00 UTC)	−0.9	0.02
Guadeloupe (12:00 UTC)	−0.05	0.91
Puerto Rico (00:00 UTC)	−0.26	0.61
Puerto Rico (12:00 UTC)	−0.17	0.74
Cayman Islands (00:00 UTC)	−0.45	0.44
Cayman Islands (12:00 UTC)	Insufficient data	—

AOD: aerosol optical depth; CAPE: convective available potential energy.

r = 0.13, p = 0.79 at 12:00 UTC) between AOD and CAPE values. Cayman shows a substantial drop at 00:00 UTC (r = −0.45, p = 0.44), but Guadeloupe shows a very strong negative correlation (r = −0.93, p = 0.02 at 00:00 UTC). However, the data values at 12:00 UTC were insufficient to compare this site with others. Puerto Rico, on the other hand, shows weak negative correlations at both 00:00 and 12:00 UTC, with correlation coefficients of −0.26 (p = 0.61) and −0.17 (p = 0.74), respectively. The positive correlation from the dusty-case results (r = 0.52 and 0.33, respectively) is physically notable even if neither statistical result is significant.

3.3.2 Correlation coefficient (r) between water vapor (wv) and CAPE results

This section summarizes the statistical findings when both moisture and dust are present (scenario 1). For dusty and low dust days, the correlation coefficients between the vertical averages of water vapor and the vertical integral CAPE values at 00:00 UTC and 12:00 UTC are displayed in Tables IV and V, respectively. Significant correlations (r = 0.85, *p*-value = 0.029) at noon in Barbados, large correlations (r = 0.90, *p*-value = 0.016) at night in Guadeloupe, and large correlations (r = 0.93, *p*-value = 0.021) at noon in the Cayman Islands indicate that the relationship between water vapor and convective instability is primarily positive during dusty conditions throughout the Caribbean. In addition, Puerto Rico also has positive correlation (r = 0.08, *p*-value = 0.054 at 00:00 UTC) but has less contribution. During low-dust conditions, correlations remain positive but are less significant compared with dusty days across all study regions and times (Table V).

Table IV. Statistical results between vertical averages of water vapor (g kg^{-1}) and CAPE (J kg^{-1}) values under dust and water vapor effects (scenario 1) for dusty days.

Sites/low dust	r	p
Barbados (00:00 UTC)	0.14	0.72
Barbados (12:00 UTC)	0.85	0.029
Guadeloupe (00:00 UTC)	0.9	0.016
Guadeloupe (12:00 UTC)	0.29	0.68
Puerto Rico (00:00 UTC)	0.08	0.054
Puerto Rico (12:00 UTC)	0.05	0.97
Cayman Islands (00:00 UTC)	0.29	0.63
Cayman Islands (12:00 UTC)	0.93	0.021

Table V. Statistical results between vertical averaged water vapor (g kg^{-1}) and CAPE (J kg^{-1}) values under dust and water vapor effects (scenario 1) for low dust days.

Sites/low dust	r	p
Barbados (00:00 UTC)	0.63	0.17
Barbados (12:00 UTC)	0.09	0.86
Guadeloupe (00:00 UTC)	0.65	0.23
Guadeloupe (12:00 UTC)	0.5	0.30
Puerto Rico (00:00 UTC)	0.05	0.92
Puerto Rico (12:00 UTC)	0.5	0.26
Cayman Islands (00:00 UTC)	0.07	0.90
Cayman Islands (12:00 UTC)	Insufficient data	—

3.3.3 Percentage differences in CAPE and CIN for dust and water vapor effects

This section provides an overview of percentage changes and percentage differences between the effects of dust with water vapor (scenario 1) and the individual effect of dust (scenario 2). The percentage variations in convective instability between dust and water vapor impacts (previously shown in Table I) and dust effect alone (scenario 2) are displayed in Table VI. The research findings for the latter impact (scenario 2) are shown in Table SI in the supplementary material. When comparing the data in Tables I and SI, the results in all research regions (percentage changes, see Table VI) for dusty days between 00:00 and 12:00 UTC, show a decrease in CAPE. With −18.11% at 00:00 UTC and −11.58% at 12:00 UTC, Barbados has the highest negative values (biggest CAPE drops) of all the Caribbean Islands. At −5.93% (00:00 UTC) and −9.78% (12:00 UTC), Guadeloupe likewise shows a notable decrease in CAPE. However, there is a striking significant reduction in percentage change records at the Cayman site with −11.22% at 00:00 UTC and −8.10% at 12:00 UTC, while Puerto Rico shows a lower percentage reduction with −3.62% at 00:00 UTC and −0.76% at 12:00 UTC (Table VI).

Figures 4, 5, S10, S11, S12, and S13 show the percentage differences between scenarios 1 and 2, quantifying how CAPE and CIN change at each atmospheric level. Most of the atmospheric column, especially above 3 km (Fig. 4), displays increased

Table VI. Average percentage change in CAPE results between scenarios 1 and 2.

Sites	Valid CAPE values	Average percentage change	Direction
Barbados (00:00 UTC)	6	−18.11%	Decrease
Barbados (12:00 UTC)	6	−11.58%	Decrease
Guadeloupe (00:00 UTC)	4	−5.93%	Decrease
Guadeloupe (12:00 UTC)	4	−9.78%	Decrease
Puerto Rico (00:00 UTC)	6	−3.62%	Decrease
Puerto Rico (12:00 UTC)	6	−0.76%	Decrease
Cayman Islands (00:00 UTC)	5	−11.22%	Decrease
Cayman Islands (12:00 UTC)	5	−8.10%	Decrease

CAPE under dust associated with water vapor on June 25 (red) compared to June 1 (black). Results reveal declines in CAPE values under vertical CAPE with reference moisture conditions, suggesting that anomalously high water vapor on June 25 exacerbates upper-tropospheric instability.

In the lower (~0.5-1 km) and upper (~1-6.5 km) troposphere, the CAPE percentage difference at Barbados on both dates ranges from ~20 to 40%, indicating that moisture contributes to convective instability across the entire atmospheric profile. In contrast to the Barbados region, Guadeloupe exhibits a low-to-moderate CAPE percentage difference of approximately 10-30% across the lower and upper troposphere, despite having no profile on June 1 at 00:00 UTC (see missing CAPE and CIN profiles for both dust scenarios in Fig. 4 [c1]). Convective inhibition has low or negligible values in the lower atmosphere for the dates and times of Barbados and Guadeloupe locations, despite CIN reaching a peak (exceeding 80%) at altitudes less than 0.5 km on June 1 (Fig. 4). Compared to Barbados and Guadeloupe, Puerto Rico exhibits a clear vertical structure in Figure 5, especially at night on June 1. CAPE values are widely dispersed throughout the column, but above 5 km they rise dramatically to about 150-175 J kg^{-1}. At 00:00 UTC on June 1 (black), vertical CAPE shows a more uniform structure with residual values of about 50 J kg^{-1}; however, the structure pattern flips at 12:00 UTC on June 1 (black). With doubled-peak percentage changes (~30-40%) between ~1 and 2.5 km, scenarios 1 and 2 track closely on both dates and times. A more consistent difference of approximately 15-25% between 0.5 and 3 km, and approximately 5-10% above 4 km, is observed in the percentage difference on June 25 (red).

Barbados displays a more significant CAPE structure on June 26 and 27 at 00:00 UTC with around 100-150 J kg^{-1} above approximately 3 km (Fig. S10). On June 27, CAPE displays a peak (~200 J kg^{-1}) above 4 km at 12:00 UTC. In the lower atmosphere (less than 1 km), percentage differences in June (black) at 12:00 UTC reach roughly 40-50%. Guadeloupe, on the other hand, exhibits a different CAPE structure. The June 25 difference is not substantial below 1.5 km, but it gradually grows to about 50-80% between about 3 and 6 km. The percentage difference indicates that the combination of dust and water vapor causes a greater increase (~20-30 J kg^{-1}) than the dust effect alone, indicating that moisture increases upper-level instability during summer daylight. Guadeloupe exhibits a peak percentage difference of about 35-40% in the lower atmosphere at 12:00 UTC on June 26 (black) and 27 (red), although it rises to values between 70-100% at 1.5-2 km before falling to about 10% in the high atmosphere. On the other hand, between approximately 0.4 and 0.6 km, the percentage difference in CIN is about 80% (blue line, June 1 reference). The CAPE profiles (scenarios 1 and 2) at Puerto Rico and Cayman (Fig. S11) during June 26-27 track closely again at lower levels but diverge at the upper atmosphere (> 4 km), where dust and water vapor exhibit higher CAPE (~30-50 J kg^{-1}) than the dust effect alone on June 26. At elevations below 3 km, the percentage difference between the two dates (00:00 UTC, black) is substantial (~100%). Additionally, CIN exhibits a significant (~80-90%) variation between ~0.3 and 0.5 km, although it displays a minor convective inhibition across the whole column. Moisture leads to convective instability in the upper atmosphere at Cayman, especially around

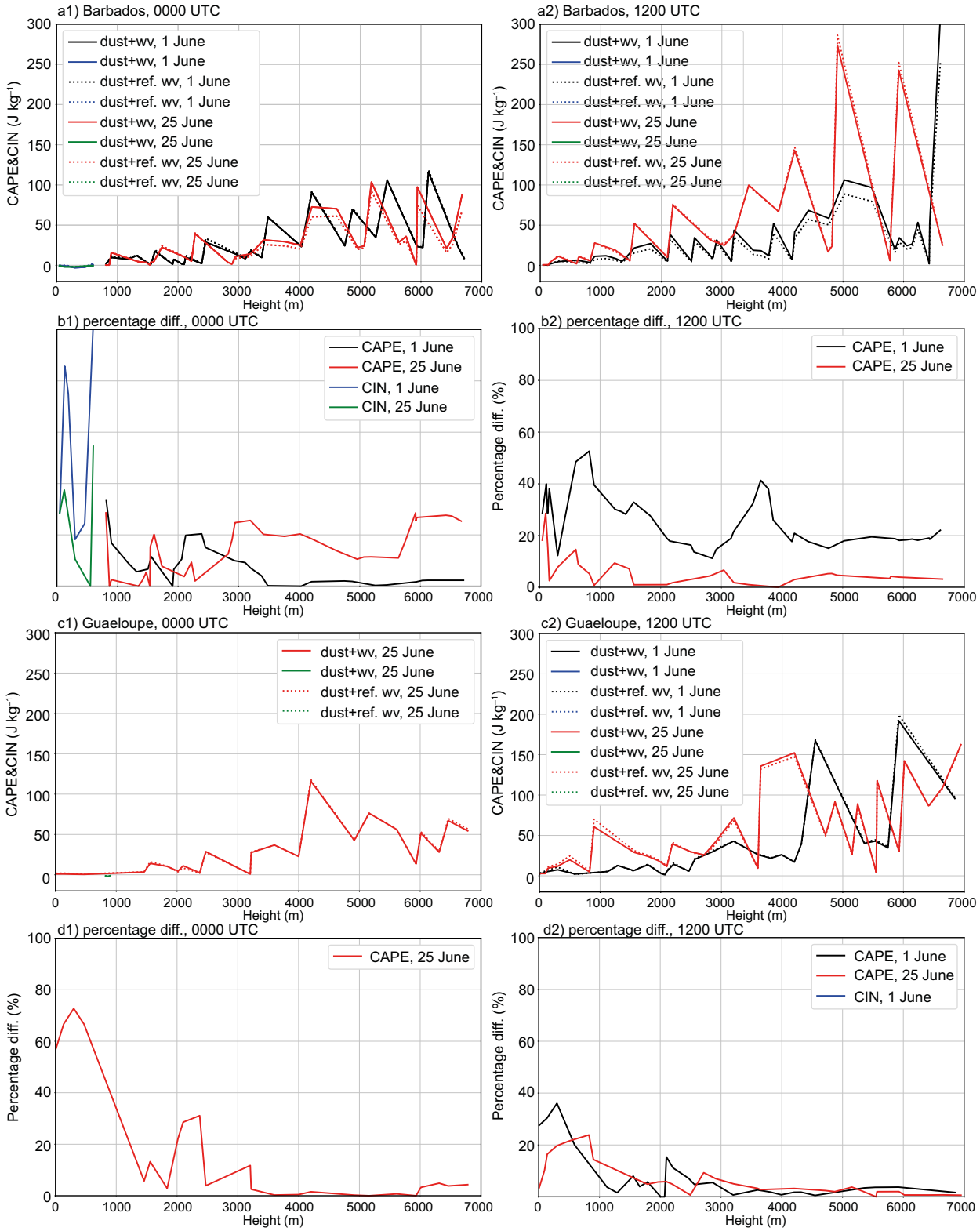

Fig. 4. Within two dusty days (June 1 and 25, 2024), CAPE and CIN values were calculated for Barbados (case A) and Guadeloupe (case B) at 00:00 UTC (first column, a1-c1) and 12:00 UTC (second column, a2-c2). Black and red dashed lines display values with dust using midlatitude-referenced water vapor during summer (wv); black and red solid lines show CAPE and CIN results, including both dust and water vapor. Percentage differences (%) between dust with water vapor and dust with background water vapor are displayed in the second and fourth rows, respectively, for CAPE and CIN results in cases (A) and (B). In all percentage difference plots, CAPE results for dusty days (June 1 and 25) are shown with black and red lines, while the differences in CIN percentages are displayed in the second and fourth rows, respectively, with blue and green lines. (CAPE: convective available potential energy; CIN: convective inhibition; wv: water vapor.)

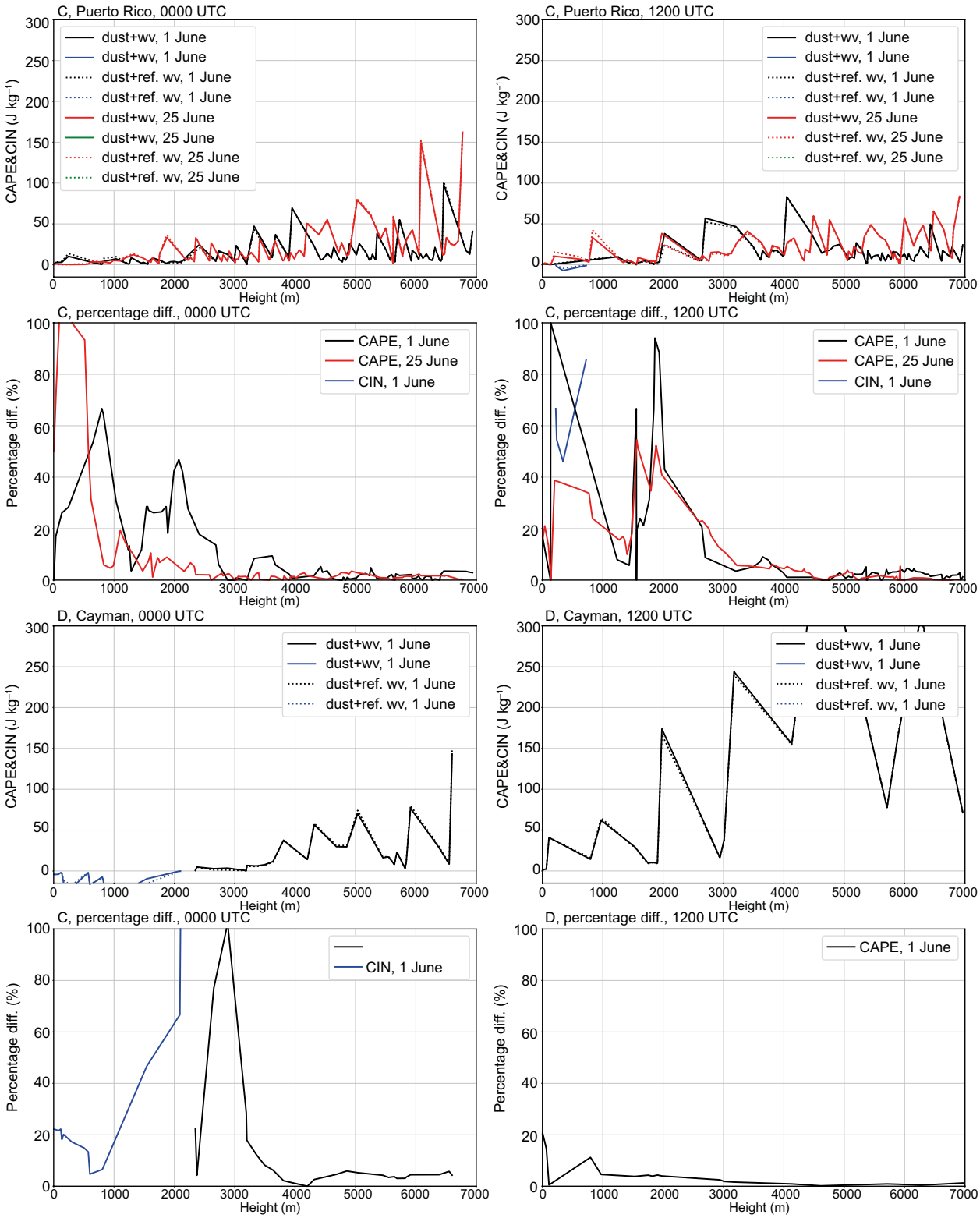

Fig. 5. As in Figure 4, but for Puerto Rico and the Cayman Islands.

00:00 UTC on June 27. At 12:00 UTC, it rises to a peak of ~200-225 J kg^{-1} near 4 km, despite low vertical CAPE values on some dates. Under dust and water vapor impacts, CAPE shows greater values than dust alone at about 2.5 km on June 26. The percentage difference exceeds ~80% below ~500 m, but it then drastically decreases to ~25% between this level and up to 2 km. On June 1, CIN displays a large percentage difference (~50-60%) below 0.5 km.

The aforementioned findings indicate that convective instability may be influenced by water vapor rather than just dust. This is in line with the impact of moisture content in Barbados on May 18 and 19 (Fig. S12 in the supplementary material), with percentage differences of ~20-50% at 12:00 UTC and ~55-65% at ~0.5-2.5 km at 00:00 UTC. On May 18, however, the percentage difference is dominating at 12:00 UTC compared to 00:00 UTC, peaking at about 65-70% between 0.5 and 0.8 km. Additionally, Figure S13 demonstrates that Cayman displays a distinct structure at 12:00 UTC with a high CAPE (~200-225 J kg^{-1}) around 5-6 km, whereas Puerto Rico contributes to a high CAPE value on both days.

4. Discussions

For all profiles, water vapor and relative humidity begin at high levels at the surface and then rise sharply at the inversion layer, located at an altitude of roughly 1.5 km. A thin inversion layer spanned between the inversion layer and at about 2 km. At this altitude, relative humidity and water vapor levels increase, peaking at roughly 3 km, and then decline sharply above 4 km. Our findings are consistent with earlier research that examined the highest dust levels over Barbados, including Prospero et al. (2014). The atmospheric variables of the Cayman Islands show slight vertical variation and a general decrease in structure with altitude, in contrast to other Caribbean regions.

CAPE and CIN results show significant spatio-temporal patterns of convective instability for the combined dust and water vapor effect in June, May, and September 2024. These patterns reflect the impact of Saharan dust intrusions, water vapor variability, and regional atmospheric dynamics throughout the Caribbean Islands. The vertical distributions of the CAPE and CIN profiles, which start at low values below 3 km and gradually increase above this altitude, are the most constant feature across all dates, times, and locations. This is consistent with the findings of Gilmore and Wicker (1998), who demonstrated that the downdraft convective available potential energy (DCAPE) is probably increased from 2 to 7 km. Additionally, CAPE profiles show significant vertical heterogeneity, with peak contributions occurring above 3 km, suggesting mid-tropospheric instability rather than convection driven by boundary layers. This mechanism, in which radiative heating by dust particles stabilizes the lower troposphere and strengthens CIN at low altitudes, is consistent with the comparatively lowered CAPE values near the surface (below ~1.5 km) across most profiles.

Compared with the vertical structure of convective instability across the column, integrated vertical CAPE and CIN may provide a more straightforward and distinct explanation. The region's sensitivity to the SAL is confirmed in Table I, which shows a range of stability regimes in the link between AOD and convective instability. The lack of a weak inverse association between AOD and CAPE during dusty events is a crucial finding, but the opposite relationship is evident on days with little dust. For example, in Puerto Rico on May 18 at 12:00 UTC, the greatest CAPE value (2287 J kg^{-1}) corresponds to a moderate AOD of 0.4, indicating that deep convection can continue even in moderately murky conditions if there is enough moisture available. On the other hand, a comparable AOD of 0.3 is linked to a noticeably low CAPE (270.8 J kg^{-1}) at Guadeloupe on June 9 at 00:00 UTC, indicating reduced convective instability.

Due to their locations in the eastern and central Caribbean, Barbados and Puerto Rico frequently encounter direct SAL intrusions. On dusty days, a wide CAPE range (~700-2300 J kg^{-1}) is expected. However, despite low AOD (AOD = 0.2), the far western Cayman Islands nonetheless exhibit a large contribution of high CAPE (1862 J kg^{-1}), indicating that local maritime moisture can predominate over aerosol impacts when the dust plume is aged or diluted. Regardless of AOD levels, temporal variability indicates that CAPE generally rises by midday due to daytime heating. Dust load appears to regulate this increase; compared to clean mornings, high-AOD mornings frequently exhibit decreased afternoon CAPE growth.

Nevertheless, statistical research demonstrates that the combined impact of water vapor and dust on air stability is interactive rather than additive (Table II). The amount of moisture present, the height of the aerosol layer, and the time of day all influence how much dust suppresses convection. The Cayman Islands' notable—although weak—negative correlation around 12:00 UTC indicates that the stabilizing impact of dust is most noticeable in settings with an older air mass and fewer local thermodynamic disparities. These results highlight the 'necessity for process-based studies that take into account the atmosphere's vertical structure instead of depending just on column-integrated AOD to forecast convective outcomes in the dusty Caribbean atmosphere. In contrast, Table III exhibits the correlation coefficients between convective potential (when the direct radiative effects of heavy dust are absent) and the residual aerosols. The results present a striking contrast to the dusty-day analysis, particularly in the eastern Caribbean.

Thus, modulating the thermodynamic structure for the convective instability process is a valuable diagnostic for comprehending how dust and water vapor (scenario 1) differ from the dust effect (scenario 2). The moisture-CAPE correlation varies during dusty conditions, ranging from almost zero ($r = 0.05$ at Puerto Rico, 12:00 UTC) to very strong ($r = 0.93$ at Cayman, 12:00 UTC), with only three sites/times (Barbados at 12:00 UTC, Guadeloupe at 00:00 UTC, and the Cayman Islands at 12:00 UTC) achieving statistical significance. The associations are typically moderate to strong under low-dust conditions (Table V), although none of them reach statistical significance at the $p < 0.05$ level. CAPE is significant in Barbados and Guadeloupe at 12:00 UTC with $r = 0.85$ ($p = 0.029$), $r = 0.29$ ($p = 0.68$), and at 00:00 UTC with $r = 0.14$ ($p = 0.72$), $r = 0.9$ ($p = 0.016$), respectively. This suggests that the vertical alignment of moisture and dust is crucial.

However, measuring percentage changes in CAPE across various forcing scenarios provides a clear indication of how sensitive Caribbean air stability is to moisture availability and aerosol loading. Across all locations and times, the percentage shift in Table VI from the combined impact of dust and water vapor to the dust effect alone is negative. Puerto Rico displays a huge percentage change of −0.76 during noon time, while Barbados shows a significant change (−18.11%) at night. Furthermore, Cayman exhibits an intriguing decrease of −11.22% at 00:00 UTC in the far west, suggesting that the ancient dust plume still has a discernible thermodynamic impact, most likely due to its influence on mid-level moisture and stability. This uniform decrease suggests that adding dust, either by itself or in conjunction with water vapor, always leads to a more stable thermodynamic environment.

Water vapor content is therefore primarily a positive driver of CAPE throughout the Caribbean Islands, even at night and early in the morning, especially during dust events in Barbados, Guadeloupe, and the Cayman Islands. However, dust can inhibit the formation of CAPE by serving as CCNs that encourage shallow, non-precipitating clouds or by lowering lapse rates or thermal forcing. The anomaly in moisture content may not have as much impact on convective instability under low-dust conditions as other parameters, such as wind shear, temperature lapse rate, or mesoscale dynamics. Additionally, September profiles (b and d plots in the third and fourth rows of Figs. S4-S7) and the summer period (June) typically exhibit larger vertical oscillations and more noticeable CAPE magnitudes, which are compatible with a more humid mid-troposphere than that of September.

Cloud formation is less common in the Caribbean Islands at night on all days, as evidenced by the fact that CIN actively occurred during 00:00 UTC rather than at 12:00 UTC, even when CIN is low or insignificant in the lower atmosphere. To explain this, the temperature of the air parcel will rise during the day as solar radiation warms the Earth's surface. A well-mixed convective planetary boundary layer is produced when this energy is transferred to the surrounding air just above. The air becomes less thick and more buoyant in this scenario, suggesting a decrease in CIN at noon. On the other hand, at night, the radiative cooling effect (long-wave radiation emitted) results in denser air, which forces it to descend and form a stable layer (an inversion layer) close to the surface. Dust has a minor effect on cloud formation and precipitation below the inversion layer, but it has little effect on blocking convection compared to moisture.

5. Conclusions

Three statistically significant positive WV-CAPE correlations emerged only during dusty periods

(Barbados at 12:00 UTC, Guadeloupe at 00:00 UTC, and Cayman at 12:00 UTC), indicating that water vapor is a significantly stronger predictor of CAPE under dusty conditions than under low-dust conditions. This result is consistent with the theory that dust suppresses convective instability in the Caribbean troposphere and interacts with atmospheric moisture in the Sahara to modulate it. These findings emphasize the importance of accounting for aerosol–moisture interactions when evaluating convective potential in dust-affected areas.

The percentage change analysis shows that the combined effect of Saharan dust and the resulting water vapor depletion consistently and significantly lowers CAPE at all four Caribbean stations. The suppression ranges from −0.76 to −18.11%, which is consistent with the dust transport pathway gradually decreasing from Barbados to Puerto Rico. With significant ramifications for tropical cyclogenesis forecasting during busy dust seasons, these findings highlight the dual role of Saharan dust as a direct radiative influence and an indirect moisture modifier in limiting Caribbean convective instability.

Water vapor anomalies linked to Saharan dust events contribute 15-65% of the total CAPE signal across the vertical column at both Barbados and Guadeloupe, according to the percentage difference analysis. This confirms that Saharan dust modulates Caribbean convective instability not only through direct aerosol radiative effects but also, critically, through the co-transport of anomalously dry or moist air masses. Accurate convective forecasting during dust intrusion events requires separating these contributions.

The best way to characterize the combined impact of dust and water vapor on Caribbean air stability is as a moisture-driven system influenced by aerosol forcing. Convection is fueled by water vapor, and dust acts as a thermodynamic brake whose effectiveness depends on the aerosol layer's concentration, vertical structure, and age. These results highlight the necessity for vertically resolved data and dust-aware parameterizations in operational models, and they have significant consequences for rainfall forecast, drought monitoring, and the evaluation of tropical cyclone potential in the area.

Acknowledgments

We acknowledge the NOAA's National Centers for Environmental Information (NCEI) for atmospheric observations based on the Integrated Global Radiosonde Archive (IGRI) observations, and NASA's MODIS-Aqua for satellite observations of AOD used in this project. In addition, we thank Anderson et al. (1986) and Gutleben et al. (2019) for the referenced water vapor data used in this work.

References

Anderson GP, Clough SA, Kneizys FX, Chetwynd JH, Shettle EP. 1986. AFGL atmospheric constituent profiles (0.120 km). No. AFGLTR860110. Air Force Geophysics Laboratory, Hanscom AFB, MA, USA.

Awoleye PO, Adebiyi AA, Abiodun BJ, Balogun IA, Akinbobola A, Oluleye A, Ajayi VO. 2025. Moisture and dust in motion: The dual role of integrated vapour transport over West Africa. Theoretical and Applied Climatology 156: 666. https://doi.org/10.1007/s00704-025-05913-1

Barreto Á, Cuevas E, García RD, Carrillo J, Prospero JM, Ilić L, Basart S, Berjón AJ, Marrero CL, Hernández Y, Bustos JJ. 2022. Long-term characterisation of the vertical structure of the Saharan Air Layer over the Canary Islands using lidar and radiosonde profiles: Implications for radiative and cloud processes over the subtropical Atlantic Ocean. Atmospheric Chemistry and Physics 22: 739-763. https://doi.org/10.5194/acp-22-739-2022

Buchard V, Da Silva AM, Colarco PR, Darmenov A, Randles CA, Govindaraju R, Torres O, Campbell J, Spurr R. 2015. Using the OMI aerosol index and absorption aerosol optical depth to evaluate the NASA MERRA Aerosol Reanalysis. Atmospheric Chemistry and Physics 15: 5743-5760. https://doi.org/10.5194/acp-15-5743-2015

Chen SH, Huang CC, Kuo YC, Tseng YH, Gu Y, Earl K, Chen CY, Choi Y, Liou KN. 2021. Impacts of Saharan mineral dust on air-sea interaction over north Atlantic Ocean using a fully coupled regional model. Journal of Geophysical Research: Atmospheres 126: e2020JD033586. https://doi.org/10.1029/2020JD033586

Dunion JP, Velden CS. 2004. The impact of the Saharan air layer on Atlantic tropical cyclone activity. Bulletin of the American Meteorological Society 85: 353-366. https://doi.org/10.1175/BAMS-85-3-353

Durán-Quesada AM, Gimeno L, Amador JA, Nieto R. 2010. Moisture sources for Central America: Identification of moisture sources using a Lagrangian analysis technique. Journal of Geophysical Research: Atmospheres 115: D05103. https://doi.org/10.1029/2009JD012455

Durre I, Vose RS, Wuertz DB. 2006. Overview of the integrated global radiosonde archive. Journal of Climate 19: 53-68. https://doi.org/10.1175/JCLI3594.1

Durre I, Yin X, Vose RS, Applequist S, Arnfield J. 2018. Enhancing the data coverage in the integrated global radiosonde archive. Journal of Atmospheric and Oceanic Technology 35: 1753-1770. https://doi.org/10.1175/JTECH-D-17-0223.1

Flores A, Sakai RK, Joseph E, Nalli NR, Smirnov A, Demoz B, Morris VR, Wolfe D, Chiao S. 2023. On Saharan air layer stability and suppression of convection over the northern tropical Atlantic: Case study analysis of a 2007 dust outflow event. Atmosphere 14: 707. https://doi.org/10.3390/atmos14040707

Gilmore MS, Wicker LJ. 1998. The influence of midtropospheric dryness on supercell morphology and evolution. Monthly Weather Review 126: 943-958. https://doi.org/10.1175/1520-0493(1998)126%3C0943:TIOMDO%3E2.0.CO;2

Giménez J, Pastor C, Castañer R, Nicolás J, Crespo J, Carratalá A. 2010. Influence of Saharan dust outbreaks and atmospheric stability upon vertical profiles of size-segregated aerosols and water vapor. Atmospheric Environment 44: 338-346. https://doi.org/10.1016/j.atmosenv.2009.10.032

Gutleben M, Groß S, Wirth M, Emde C, Mayer B. 2019. Impacts of water vapor on Saharan air layer radiative heating. Geophysical Research Letters 46: 14854-14862. https://doi.org/10.1029/2019GL085344

Gutleben M, Groß S, Wirth M, Mayer B. 2020. Radiative effects of long-range-transported Saharan air layers as determined from airborne lidar measurements. Atmospheric Chemistry and Physics 20: 12313-12327. https://doi.org/10.5194/acp-20-12313-2020

Gutleben M, Groß S. 2021. Turbulence analysis in long-range-transported Saharan dust layers with airborne lidar. Geophysical Research Letters 48: e2021GL094418. https://doi.org/10.1029/2021GL094418

Gutleben M, Groß S, Heske C, Wirth M. 2022. Wintertime Saharan dust transport towards the Caribbean: An airborne lidar case study during EUREC4A. Atmospheric Chemistry and Physics 22: 7319-7330. https://doi.org/10.5194/acp-22-7319-2022

Holben BN, Eck TF, Slutsker I, Tanré D, Buis JP, Setzer A, Vermote E, Reagan JA, Kaufman YJ, Nakajima T, Lavenu F, Jankowiak I, Smirnov A. 1998. AERONET—A federated instrument network and data archive for aerosol characterization. Remote Sensing of Environment 66: 1-16. https://doi.org/10.1016/S0034-4257(98)00031-5

Holton JR, ed. 2004. An introduction to dynamic meteorology. Elsevier Academic Press, 303 pp.

Huneeus N, Schulz M, Balkanski Y, Griesfeller J, Prospero J, Kinne S, Bauer S, Boucher O, Chin M, Dentener F, Diehl T, Easter R, Fillmore D, Ghan S, Ginoux P, Grini A, Horowitz L, Koch D, Krol MC, Landing W, Liu X, Mahowald N, Miller R, Morcrette J-J, Myhre G, Penner J, Perlwitz J, Stier P, Takemura T, Zender CS. 2011. Global dust model intercomparison in AeroCom phase I. Atmospheric Chemistry and Physics 11: 7781-7816. https://doi.org/10.5194/acp-11-7781-2011

Jury MR. 2017. Caribbean air chemistry and dispersion conditions. Atmosphere 8: 151. https://doi.org/10.3390/atmos8080151

Khan PI, Ratnam DV, Prasad P, Basha G, Jiang JH, Shaik R, Ratnam MV, Kishore P. 2022. Observed climatology and trend in relative humidity, CAPE, and CIN over India. Atmosphere 13: 361. https://doi.org/10.3390/atmos13020361

Kok JF, Adebiyi AA, Albani S, Balkanski Y, Checa-Garcia R, Chin M, Colarco PR, Hamilton DS, Huang Y, Ito A, Klose M, Li L, Mahowald NM, Miller RL, Obiso V, Pérez García-Pando C, Rocha-Lima A, Wan JS. 2021. Contribution of the world's main dust source regions to the global cycle of desert dust. Atmospheric Chemistry and Physics 21: 8169-8193. https://doi.org/10.5194/acp-21-8169-2021

Linders T, Saetra Ø. 2010. Can CAPE maintain polar lows? Journal of the Atmospheric Sciences 67: 2559-2571. https://doi.org/10.1175/2010JAS3131.1

Lurduy Sabogal G. 2021. Impact of a strong Saharan dust outbreak in the Caribbean. B.Sc. thesis. University of Barcelona.

Mote TL, Ramseyer CA, Miller PW. 2017. The Saharan air layer as an early rainfall season suppressant in the eastern Caribbean: The 2015 Puerto Rico drought. Journal of Geophysical Research: Atmospheres 122: 10966-10982. https://doi.org/10.1002/2017JD026911

Prospero JM, Collard FX, Molinié J, Jeannot A. 2014. Characterizing the annual cycle of African dust transport to the Caribbean Basin and South America and its impact on the environment and air quality. Global Biogeochemical Cycles 28: 757-773. https://doi.org/10.1002/2013GB004802

Rodakoviski BR, Kok J, Chamecki M. 2023. Dust settling from turbulent layers in the free troposphere: Implications for the Saharan air layer. Journal of Geophysical Research: Atmospheres 128: e2022JD037724. https://doi.org/10.1029/2022JD037724

Rodakoviski BR. 2024. Turbulent mixing of settling dust in the Saharan Air Layer. Doctoral dissertation, University of California.

Ryder CL. 2021. Radiative effects of increased water vapor in the upper Saharan air layer associated with enhanced dustiness. Journal of Geophysical Research: Atmospheres 126: e2021JD034696. https://doi.org/10.1029/2021JD034696

Schumacher V, Setzer A, Martins V, Victorino P. 2024. Evaluation and comparison of MODIS and MISR aerosol products with ground-based monitoring stations in the Amazon Basin. Atmospheric Environment 331: 120597. https://doi.org/10.1016/j.atmosenv.2024.120597

Xi J, Wang Y, Li R, Wu B, Fan X, Ma X, Meng Z. 2026. The impact of Sahara dust aerosols on the three-dimensional structure of precipitation systems of different sizes in spring. Atmospheric Chemistry and Physics 26: 15-32. https://doi.org/10.5194/acp-26-15-2026

Zhu A. Ramanathan V, Li F, Kim D. 2007. Dust plumes over the Pacific, Indian, and Atlantic oceans: Climatology and radiative impact. Journal of Geophysical Research: Atmospheres 112: D16208. https://doi.org/10.1029/2007JD008427

Supplementary material

Figure S1 shows vertical profiles of multi-referenced water vapor from previous studies and present vertical factors of atmospheric profiles during low-dust and dusty days in the study region. Low-dust and dusty days are indicated in the figure captions. Also, they show results referenced in the water vapor profile that was used in CAPE and CIN calculations. Furthermore, the remaining CAPE and CIN profiles are shown in these figures.

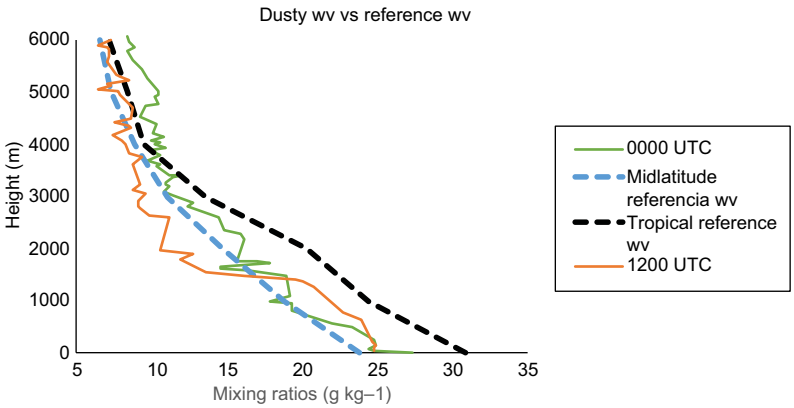

Fig. S1. Water vapor mixing ratios for a dusty event and referenced water vapor (g kg^{-1}). The blue dashed line shows midlatitude referenced water vapor profile, while the black dashed line displays tropical referenced water vapor. The orange line represents water vapor for the dusty event (June 25) at 12:00 UTC over Puerto Rico, while the green line represents water vapor at 00:00 UTC.

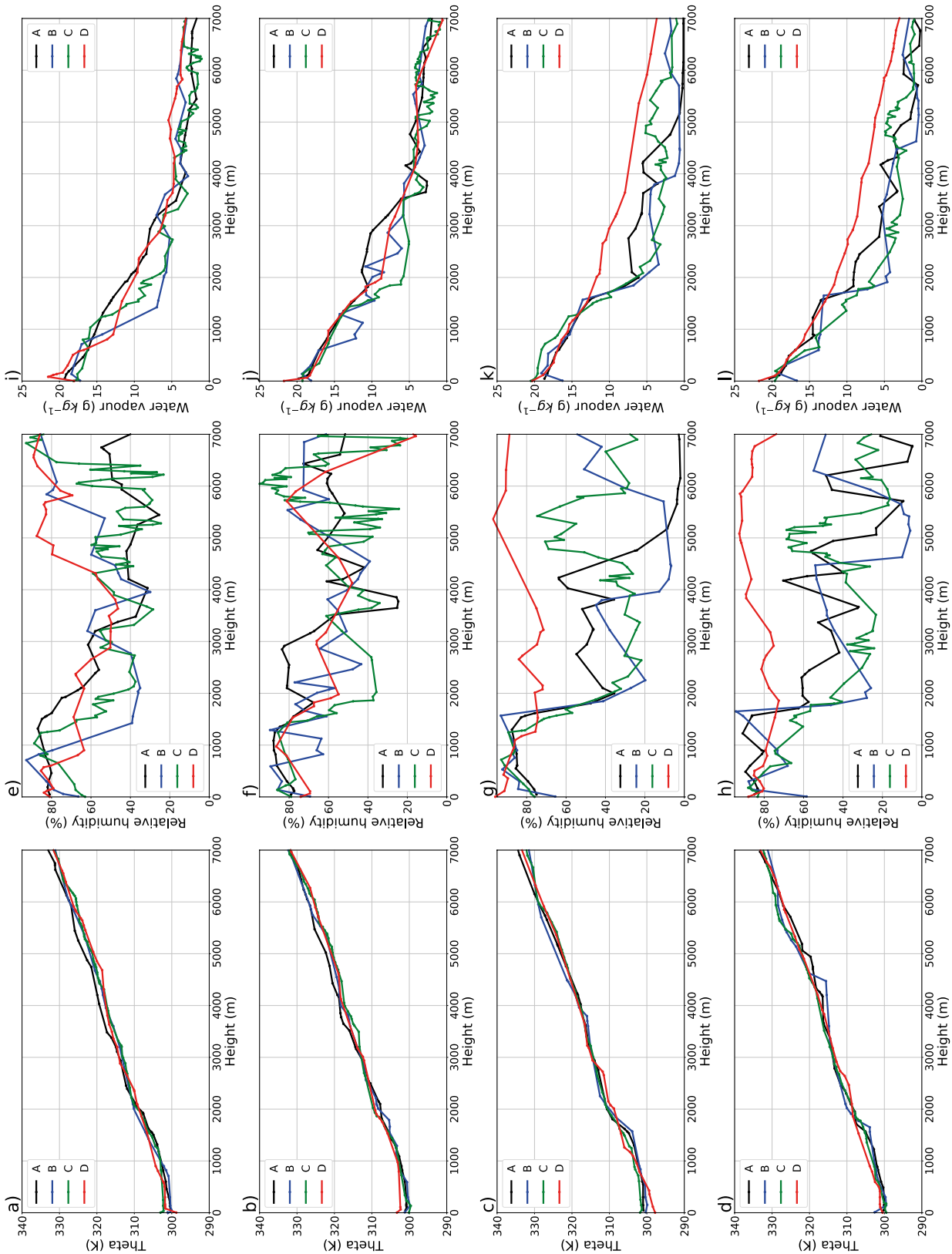

Fig. S2. Radiosonde measurements over Barbados (A, black lines), Guadeloupe (B, blue lines), Puerto Rico (C, green lines), and the Cayman Islands (D, red lines) in June 2024 between 00:00 UTC (first and third rows) and 12:00 UTC (second and fourth rows) provided a vertical profile of the atmosphere. Potential temperature (theta [a-b], Kelvin), relative humidity (e-f, %), and water vapor (i-j, g kg^{-1}) are shown for June 1 in the first (00:00 UTC) and second (12:00 UTC) rows, respectively. Likewise, the vertical profiles potential temperature (theta [c-d], Kelvin), relative humidity (g-h, %), and water vapor (k-l, g kg^{-1}), for June 9 at 00:00 and 12:00 UTC are shown in the third and fourth rows. Relative humidity in cases B and D was calculated based on Eq. (1) from radiosonde observations, since there were errors or missing values in the relative humidity.

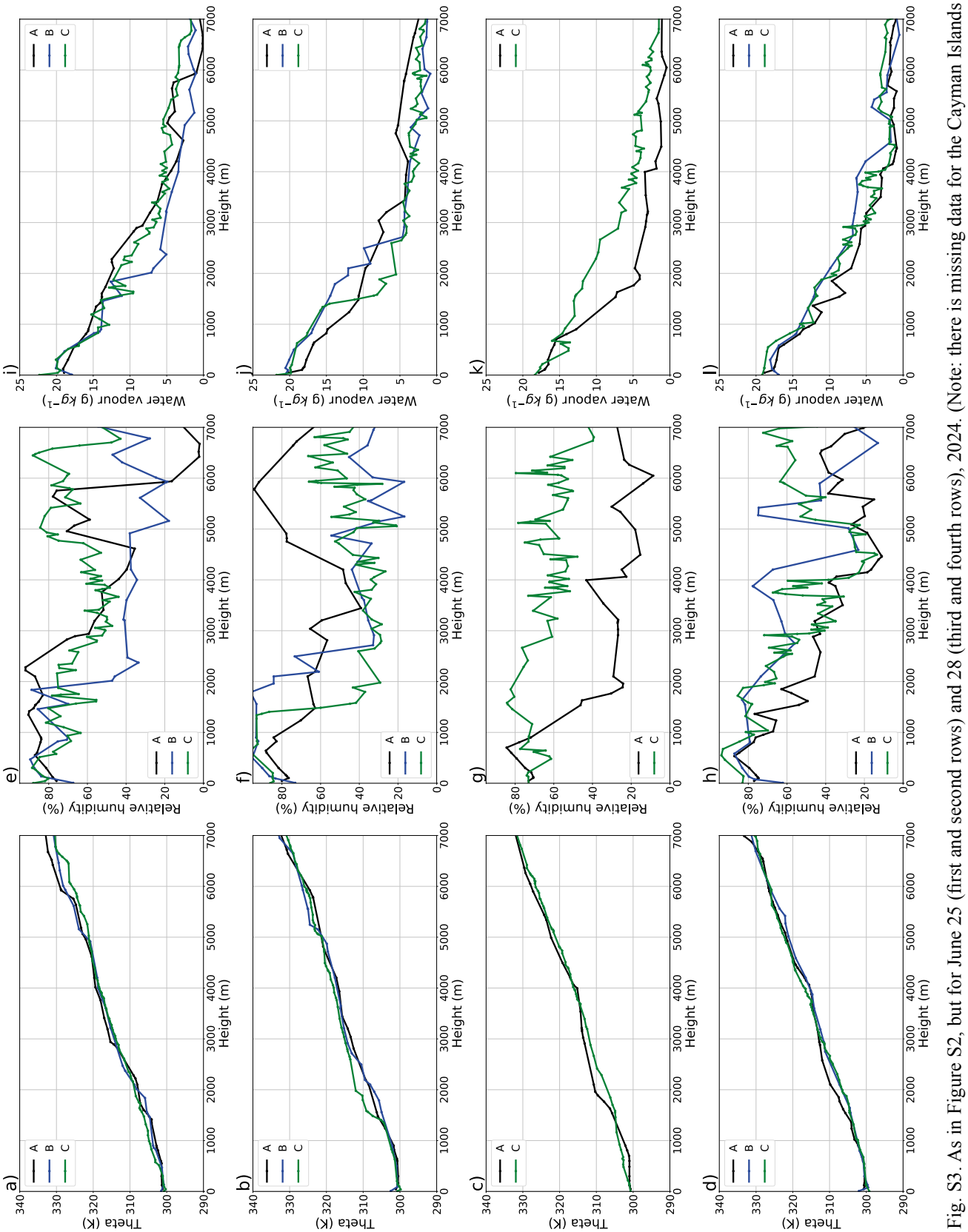

Fig. S3. As in Figure S2, but for June 25 (first and second rows) and 28 (third and fourth rows), 2024. (Note: there is missing data for the Cayman Islands [C] because radiosonde measurements were not available.)

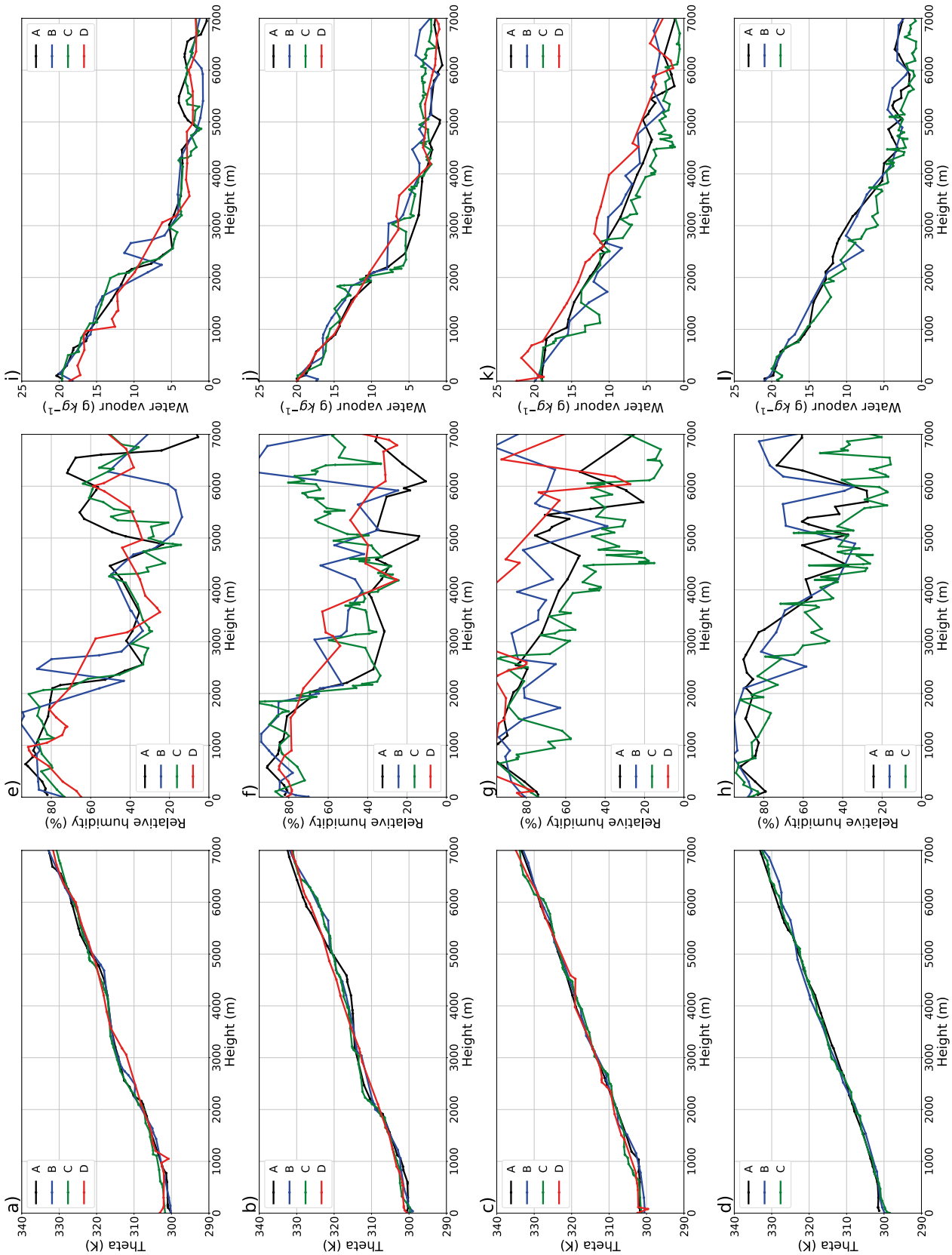

Fig. S4. As in Figure S2, but for June 26 (first and second rows) and September 12 (third and fourth rows), 2024. (Note: there is missing data for the Cayman Islands [C] because radiosonde measurements were not available.)

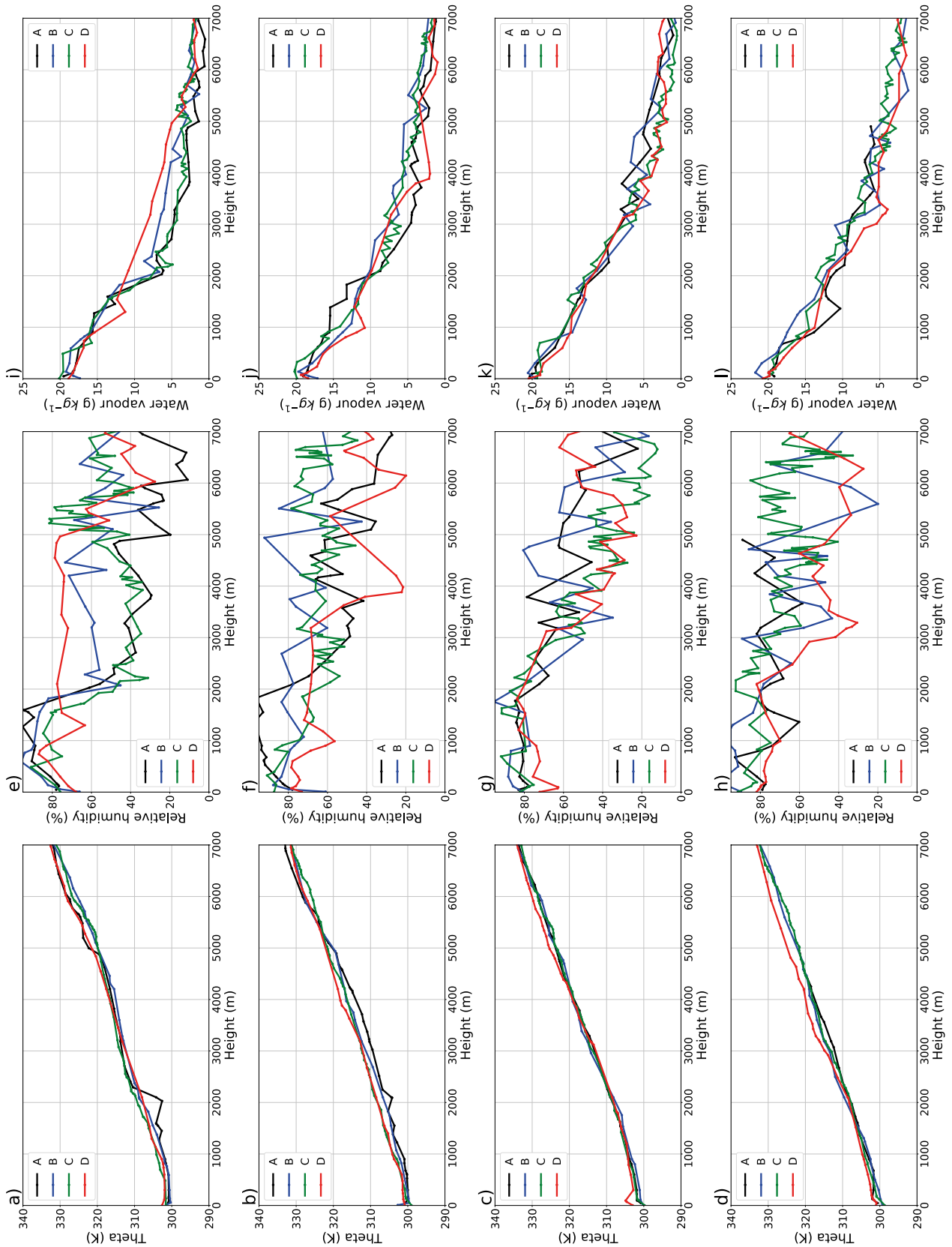

Fig. S5. As in Figure S2, but for June 27 (first and second rows) and September 13 (third and fourth rows), 2024.

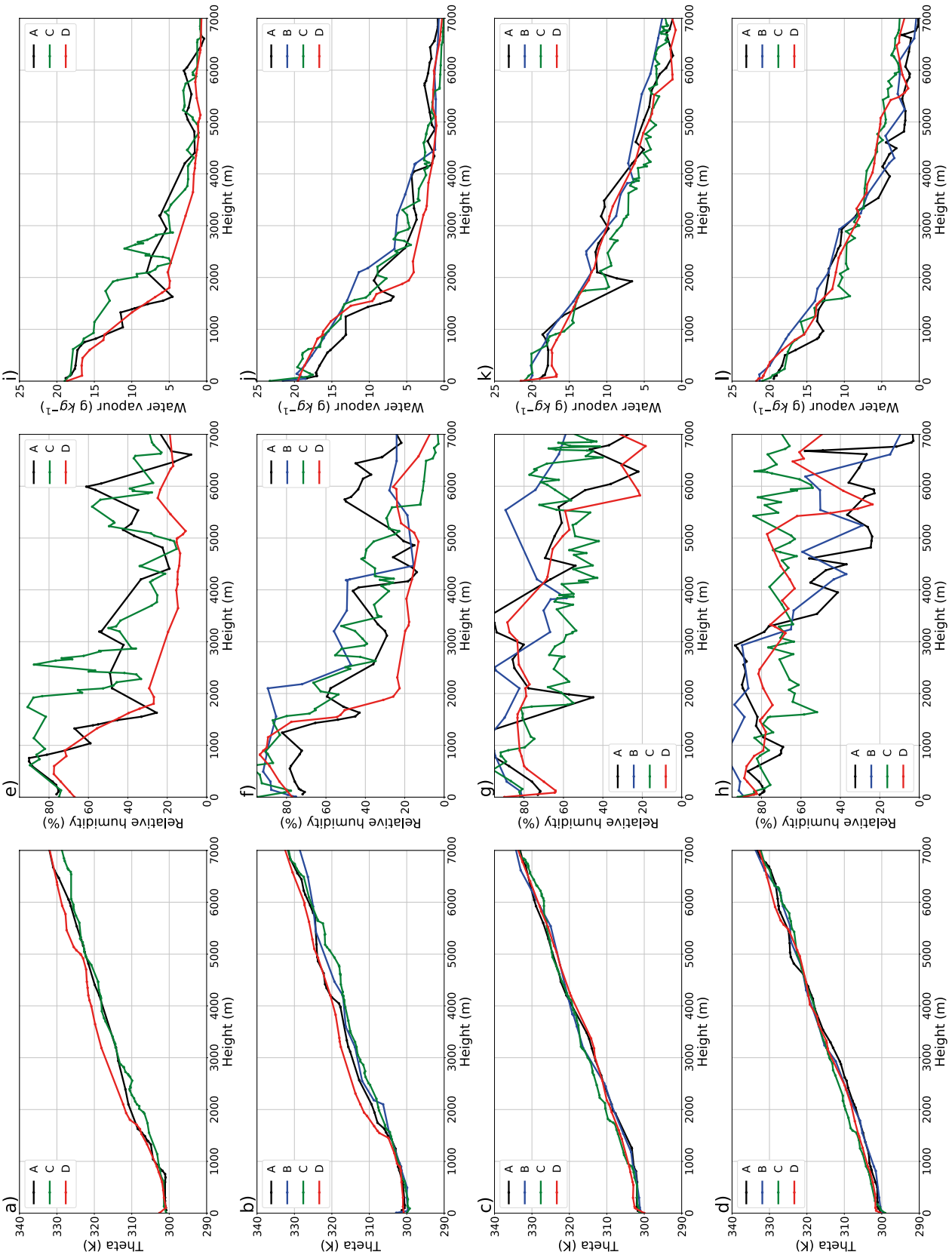

Fig. S6. As in Figure S2, but for May 18 (first and second rows) and September 14 (third and fourth rows), 2024.

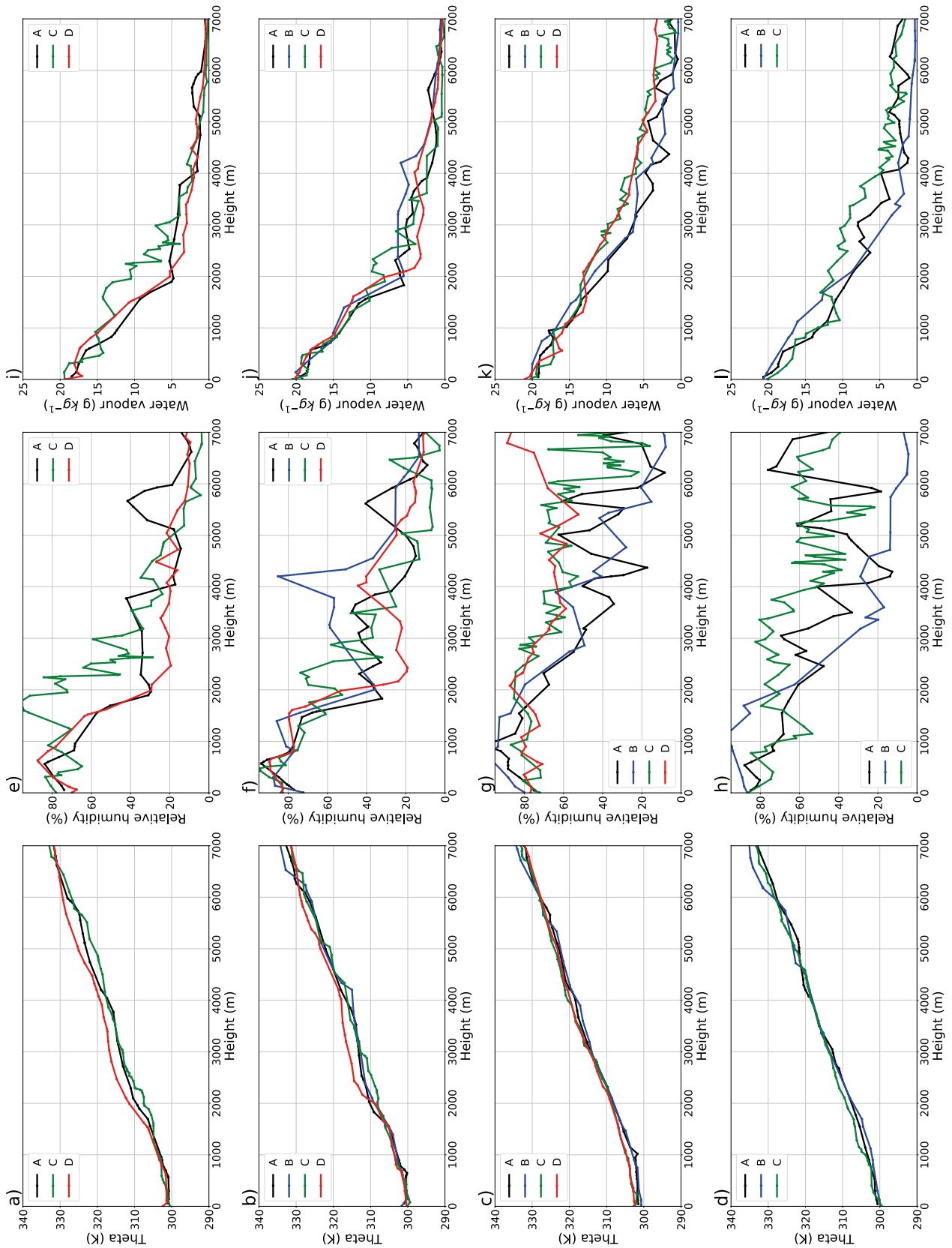

Fig. S7. As in Figure S2, but for May 19 (first and second rows) and September 15 (third and fourth rows), 2024.

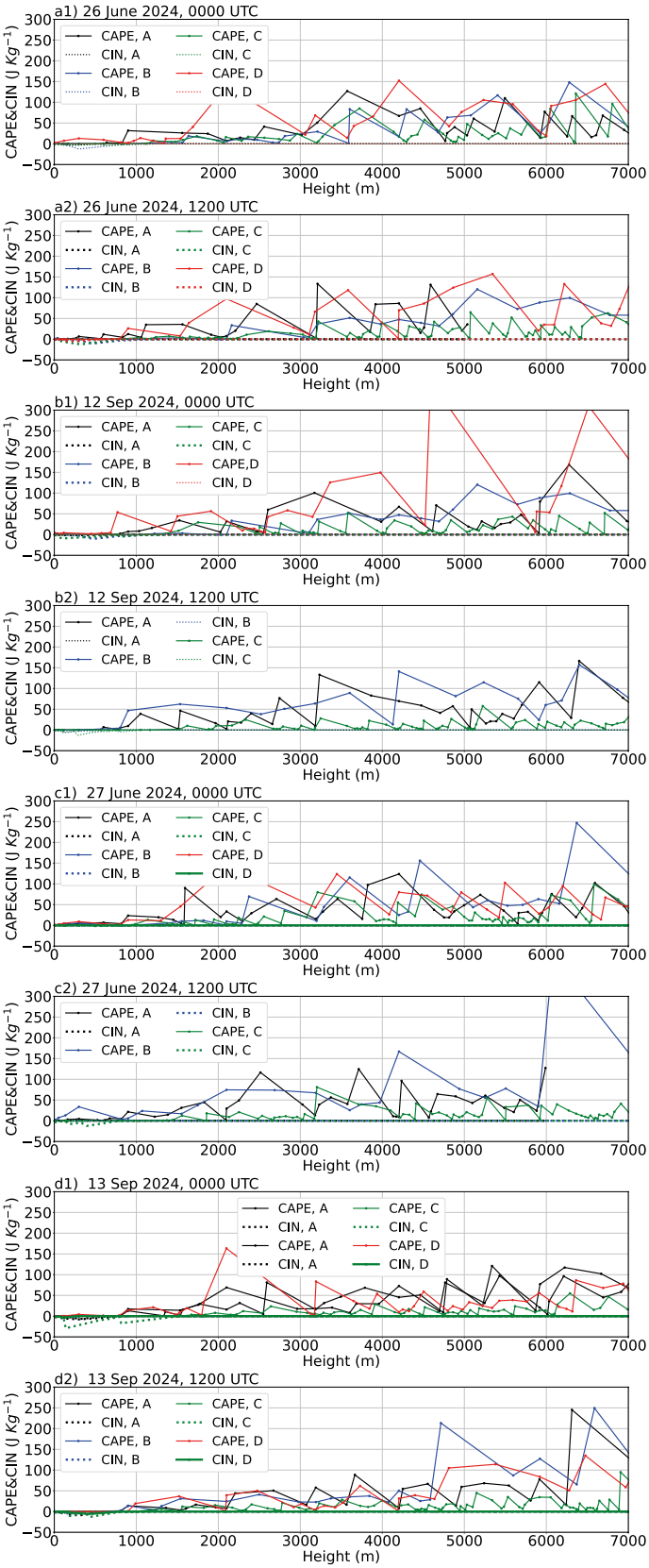

Fig. S8. CAPE and CIN vertical findings for the Caribbean Islands during June 26-27 and September 12-13,2024. Dust and water vapor were calculated for each case at 00:00 and 12:00 UTC (a1, b1, c1, d1 and a2, b2, c2, d2). CAPE values for Barbados, Guadeloupe, Puerto Rico, and the Cayman Islands are indicated by black, blue, green, and red solid lines, respectively. CIN values are represented by dashed lines. Due to an inaccuracy in the relative humidity readings from radiosonde measurements, case (D) lacks CAPE or CIN values for June 27 and September 12. (CAPE: convective available potential energy; CIN: convective inhibition.)

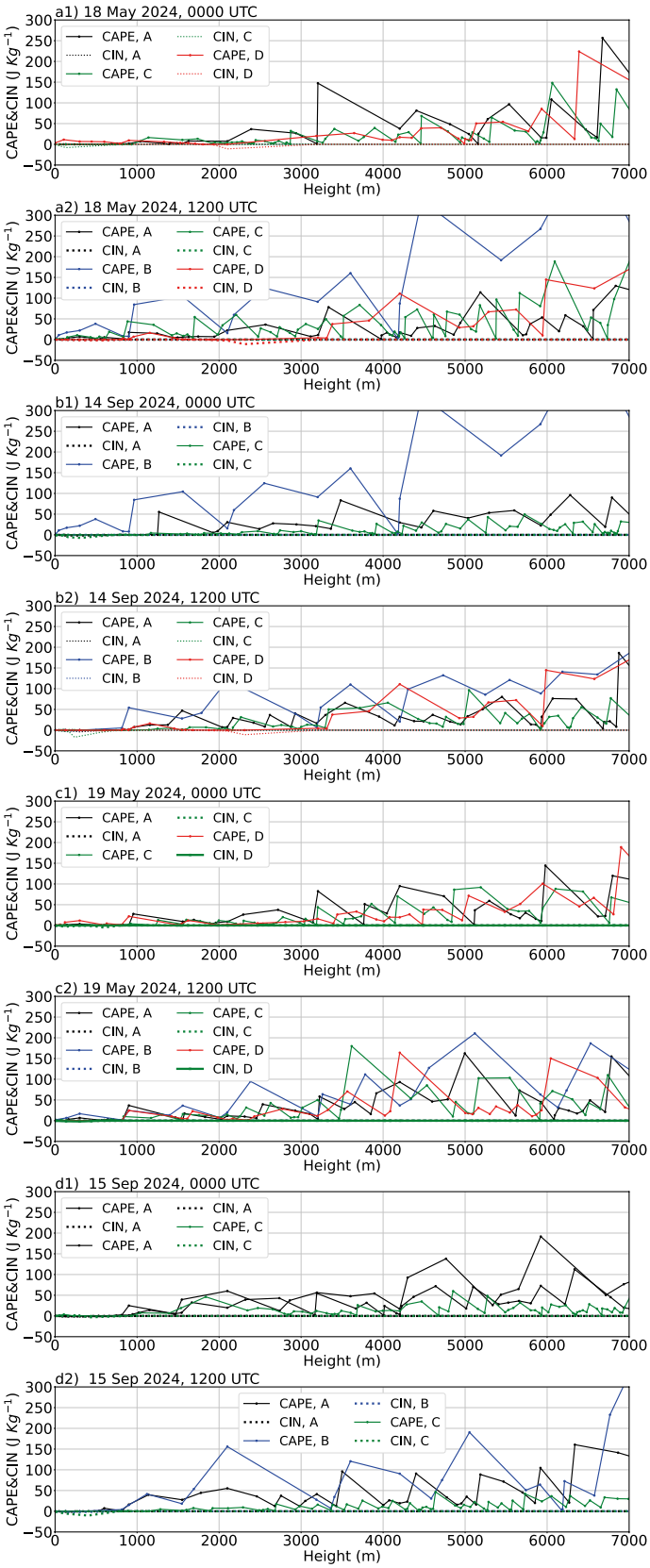

Fig. S9. As in Figure S8, but for May 18-19 and September 14-15. Due to an inaccuracy in the relative humidity readings from radiosonde measurements, case (D) lacks CAPE or CIN values for September 14-15. (CAPE: convective available potential energy; CIN: convective inhibition.)

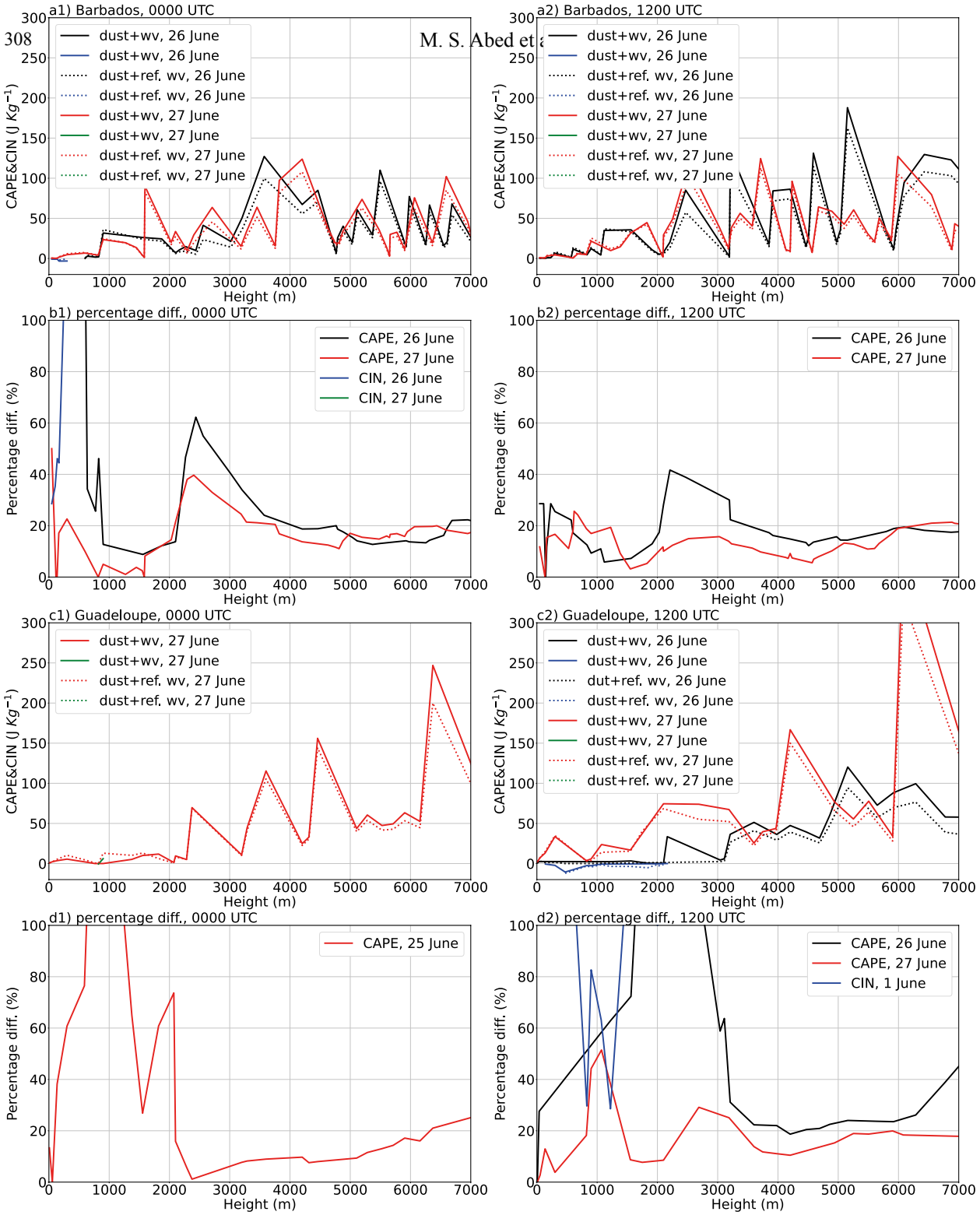

Fig. S10. Within two dusty days (June 26 and 27, 2024), CAPE and CIN values were calculated for Barbados (case A) and Guadeloupe (case B) at 00:00 UTC (first column, a1-c1) and 12:00 UTC (second column, a2-c2). Black and red dashed lines display values with dust using midlatitude-referenced water vapor during summer (wv); black and red solid lines show CAPE and CIN results, including both dust and water vapor. Percentage differences (%) between dust with water vapor and dust with background water vapor are displayed in the second and fourth rows, respectively, for CAPE and CIN results in cases (A) and (B). In all percentage difference plots, CAPE results for dusty days (June 26 and 27) are shown with black and red lines, while the differences in CIN percentages are displayed in the second and fourth rows, respectively, with blue and green lines. (CAPE: convective available potential energy; CIN: convective inhibition; wv: water vapor.)

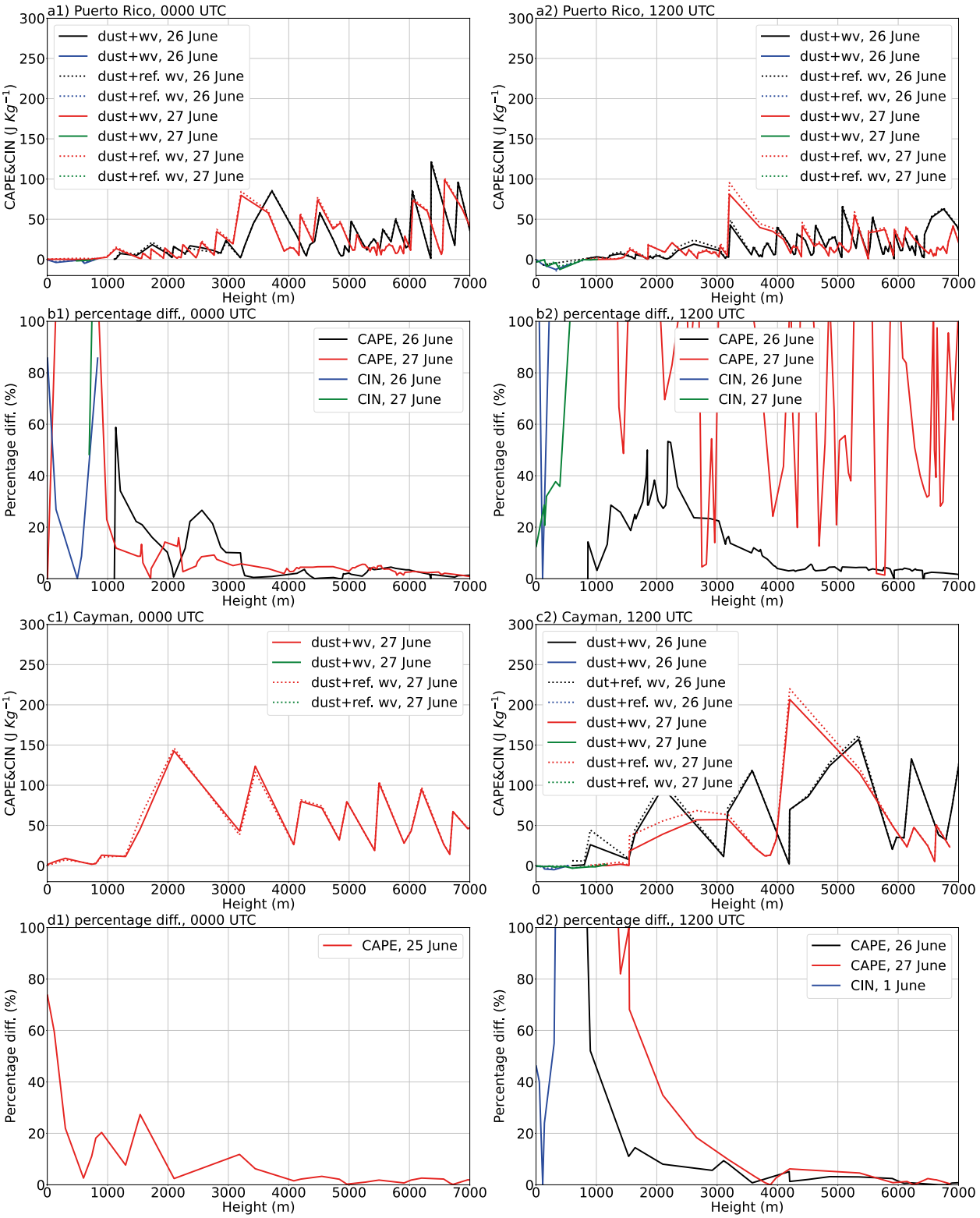

Fig. S11. As in Figure S10, but for Puerto Rico (C) and Cayman Islands (D).

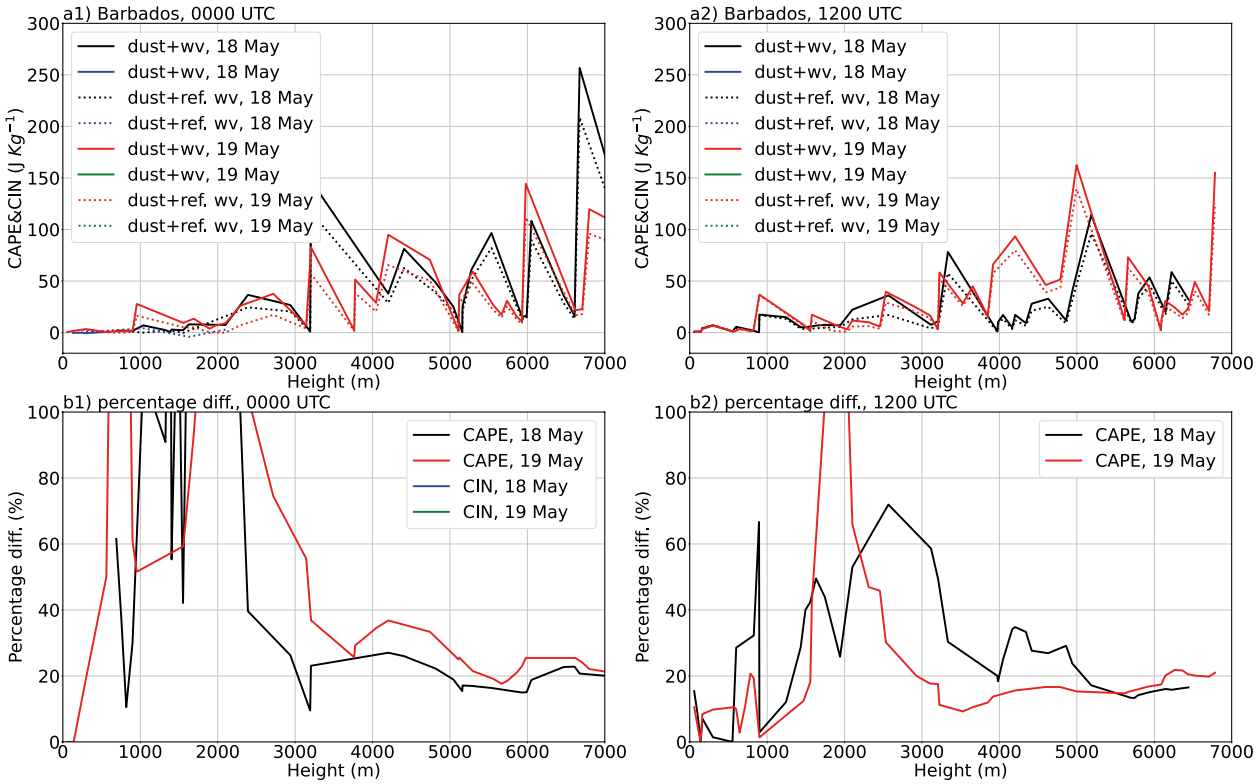

Fig. S12. As in Figure S10, but for Barbados on May 18-19.

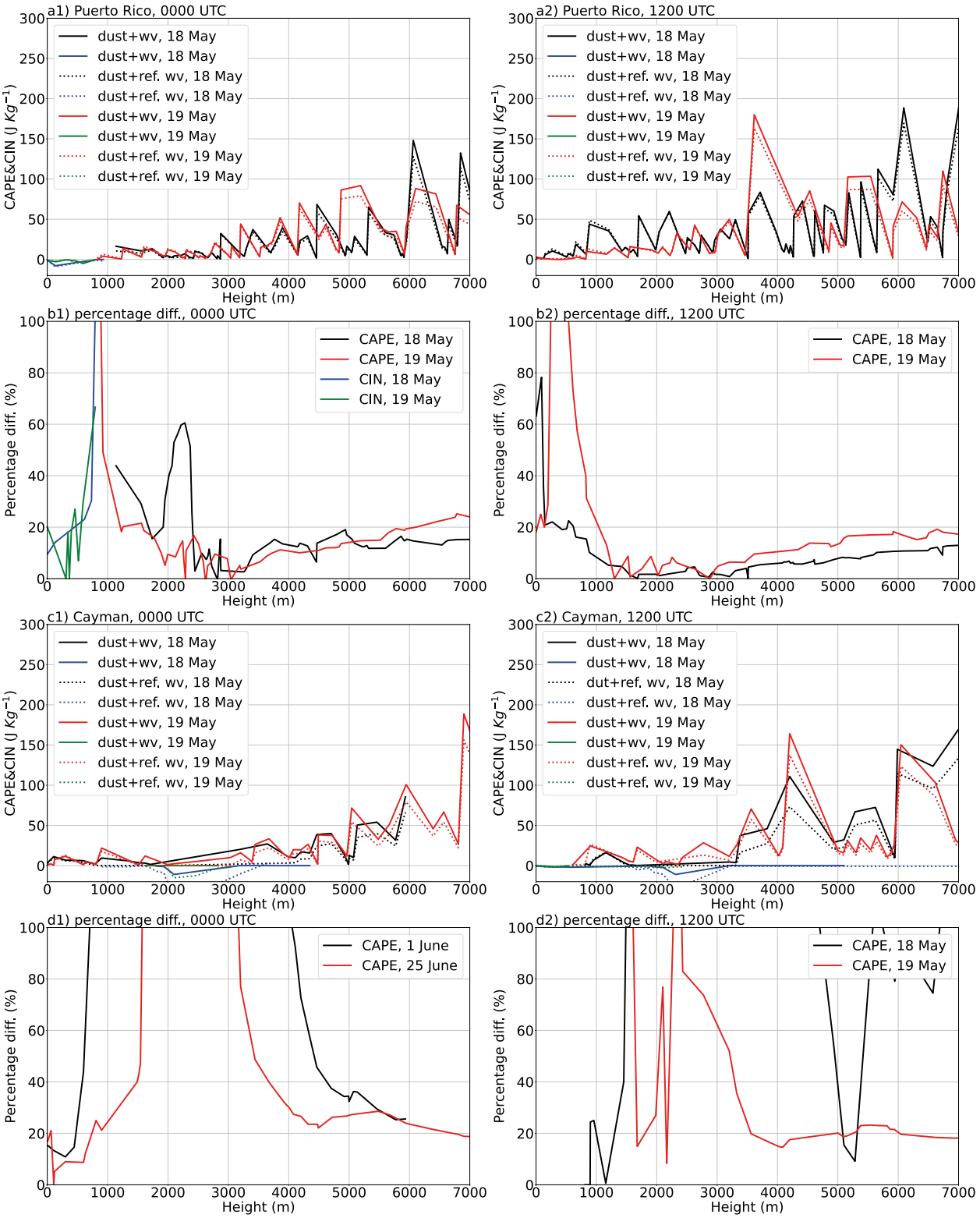

Fig. S13. As in Figure S11, but for May 18-19.

Table SI. Integrated vertical CAPE (J kg^{-1}) values under the dust effect alone (scenario 2) in each dusty day (May 18-19, June 1, 25, 26, and 27) for the Caribbean Islands.

Date, time (UTC)	Barbados		Guadeloupe		Puerto Rico		Cayman Islands	
	AOD	CAPE (J kg^{-1})	AOD	CAPE (J kg^{-1})	AOD	CAPE (J kg^{-1})	AOD	CAPE (J kg^{-1})
1 June, 00:00	0.1	799	0.2	672	0.4	1067.2	0.25	623.8
25 June, 00:00	0.3	711.9	0.5	676	0.55	1600.9	—	
26 June, 00:00	0.4	951	0.3	646	0.5	1153	0.3	1428
27 June, 00:00	0.2	1145	0.4	1007	0.3	1325	0.2	1182
18 May, 00:00	0.3	835	0.3	—	0.14	960	0.16	559
19 May, 00:00	0.3	748	0.4	—	0.26	1009	0.23	654
1 June, 12:00	0.1	1048.9	0.23	896	0.3	1015.1	0.2	1850.9
25 June, 12:00	0.3	1457.6	0.66	1611	0.55	1370	—	—
26 June, 12:00	0.4	12:00	0.4	620	0.4	1183	0.3	1263
27 June, 12:00	0.2	1277	0.3	1098	0.25	1117	0.2	934
18 May, 12:00	0.3	846	0.3	—	0.4	2153	0.19	625
19 May, 12:00	0.3	1074	0.4	—	0.45	1203	0.2	700

AOD: aerosol optical depth; CAPE: convective available potential energy.